Review

Current Progress of Magnetoresistance Sensors

Songlin Yang and Jin Zhang *

Department of Chemical and Biochemical Engineering, Western University, 1151 Richmond St., London, ON N6A 5B9, Canada; syang368@uwo.ca
* Correspondence: jzhang@eng.uwo.ca

Abstract: Magnetoresistance (MR) is the variation of a material's resistivity under the presence of external magnetic fields. Reading heads in hard disk drives (HDDs) are the most common applications of MR sensors. Since the discovery of giant magnetoresistance (GMR) in the 1980s and the application of GMR reading heads in the 1990s, the MR sensors lead to the rapid developments of the HDDs' storage capacity. Nowadays, MR sensors are employed in magnetic storage, position sensing, current sensing, non-destructive monitoring, and biomedical sensing systems. MR sensors are used to transfer the variation of the target magnetic fields to other signals such as resistance change. This review illustrates the progress of developing nanoconstructed MR materials/structures. Meanwhile, it offers an overview of current trends regarding the applications of MR sensors. In addition, the challenges in designing/developing MR sensors with enhanced performance and cost-efficiency are discussed in this review.

Keywords: magnetoresistance (MR); graphene; magnetic nanoparticles; magnetic storage; position sensing; current sensing; non-destructive monitoring; biomedical sensing; magnetoresistance (MR) sensors; graphene nanocomposites

1. Introduction

Magnetoresistance is the variation of a material's resistivity under the presence of external magnetic fields. In 1857, Lord Kelvin (William Thomson) first discovered and performed the investigation on magnetoresistance (MR) [1]. The observation of MR was 40 years ahead of the experimental discovery of electrons. In the late 1980s, two scientists discovered that the multilayer system consisting of Fe/Cr thin layers displayed large resistance changes under low temperature [2]. The MR of this Fe/Cr multilayer system under low temperature (4.2 K, $2 \times 10^1 \sim 4 \times 10^1$ kOe) was later known as the giant magnetoresistance (GMR) [3]. The discovery of GMR has dramatically boosted the development of the magnetic recording industry, especially for the advancement of hard disk drive (HDD), since IBM introduced GMR reading heads to the HDDs [4]. Nowadays, MR sensors have been broadly applied in various fields including magnetic storage/recording devices, position sensing, non-destructive monitoring, and MR biosensing platforms [4–7].

In recent years, the demands on highly-sensitive and cost-effective MR sensors raised due to the growing concerns on further improving the data storage capacity/detection sensitivity of current MR sensors and cutting down the total cost of fabrication/production, which leads to the expansion of the application area of MR sensors. Specifically, with emerging nanotechnology, the aim is to develop a novel nanomaterial that exhibits large resistance change with minimum requirements on extreme conditions (e.g., low temperatures) and large magnetic fields (>10 kOe). This work will provide a brief review of the research background of magnetoresistances (MR) and the applications of MR sensors. Meanwhile, this paper discussed current challenges in producing ideal MR sensors and the possible solution to existing difficulties. In addition, this review also explored the applications of the as-prepared materials in producing multifunctional MR sensors.

1.1. Magnetoresistance

Since the discovery of MR in 1856 by William Thomson and the observation of GMR in the 1980s, studies on investigating MR effects and materials/structures with MR are surged [1,3]. MR is defined as the phenomenon that the resistance of a material tends to change when the external magnetic fields are applied. Currently, anisotropic magnetoresistance (AMR), giant Magnetoresistance (GMR), and tunneling Magnetoresistance (TMR) have been applied in commercial applications of MR sensors [8–12].

1.1.1. Anisotropic Magnetoresistance (AMR)

In anisotropic magnetoresistance (AMR), the resistance change (ΔR) depends on the angle (θ) between the electric current and the magnetization of the metal [13]. The AMR originates from the effects of magnetization and electron spin-orbit interaction [14]. For positive AMR, the probability of s-d scattering of electrons is increased when the current direction is parallel to the magnetization direction [15,16]. In ferromagnetic metals (positive AMR, such as Ni), the maximum resistance appears when the magnetization direction is parallel to the current direction, and minimum resistance appears when magnetization is perpendicular to the current direction (Figure 1) [13]. AMR has been widely applied in the recording industry since the 1970s. The magnitude of AMR of ferromagnetic metals can be calculated by Equation (1)

$$\text{AMR} = \frac{\rho_{\parallel} - \rho_{\perp}}{\rho_{\perp}} \tag{1}$$

where $\rho_{\parallel}$ is the resistivity when current is parallel to the magnetization, and $\rho_{\perp}$ the is resistivity when the current is perpendicular to the magnetization.
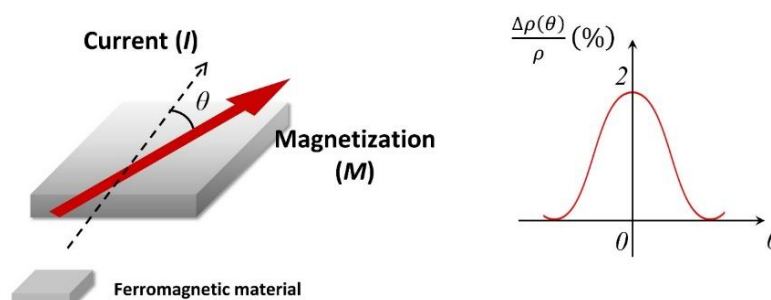

Figure 1. Schematic diagram of anisotropic magnetoresistance (AMR).

1.1.2. Giant Magnetoresistance (GMR)

Giant magnetoresistance (GMR) was discovered in the 1980s. The GMR effect was discovered in the multilayer system of Fe and Cr. The discovery of GMR initiated countless experimental or theoretical researches since GMR offers larger resistance change (ΔR) with a relatively small magnetic field, although it may require extremely low temperatures [2,3]. As shown in Figure 2, the general configuration of the magnetic multilayer system is the ferromagnetic layer/non-magnetic (or non-ferromagnetic) layer/ferromagnetic layer. GMR is related to spin-dependent scattering, which is triggered by spin-polarization of electrons under the presence of the external magnetic field [4,17,18]. The high resistances can be observed when the magnetization of two ferromagnetic layers is anti-parallel, and the low resistance state can be observed when the magnetizations are at a parallel state. The discovery of GMR has significantly increased the storage capacity of magnetic storage devices such as HDDs [4].

1.1.3. Tunneling Magnetoresistance (TMR)

Soon after the discovery of GMR, tunneling magnetoresistance (TMR) comes to the horizon of the research. TMR uses a similar magnetic multilayer configuration as the GMR. The basic unit of the TMR multilayer system is the magnetic tunnel junction (MTJ),

which follows the structure of ferromagnetic metal/insulator/ferromagnetic metal. The insulator layer is applied instead of the non-magnetic layer of the GMR multilayer system (Figure 3) [19]. The electrons can tunnel from one side of the insulator to another side due to the quantum tunnelling phenomenon [20]. The orientations of the ferromagnetic layers' magnetizations are important in TMR owing to the spin-dependent tunneling. In spin-dependent tunneling, the electron can tunnel into the subband with the same spin direction. The change of magnetizations can exchange the two spin subbands (due to the spin-polarization), which leads to the change of resistance [20]. TMR achieves relatively large resistance changes (ΔR, 30%) even in the early development stages, although extreme conditions (such as low temperature) are required [19].
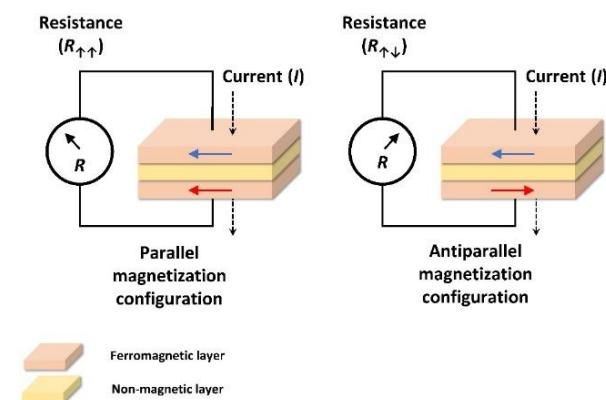

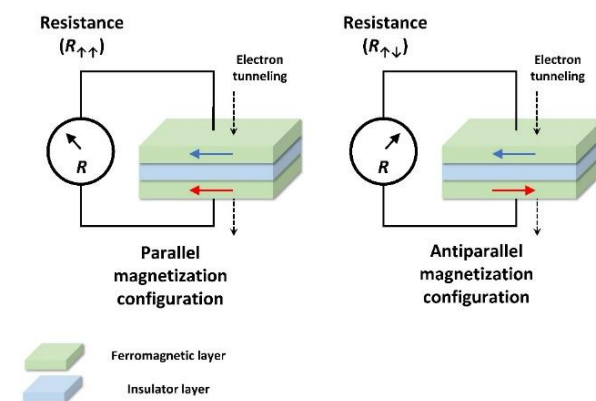**Figure 2.** Schematic diagram of giant magnetoresistance (GMR).

Figure 3. Schematic diagram of tunneling magnetoresistance (TMR).

2. Developing Magnetoresistance Materials/Structures

Since the discovery of MR, various MR materials/structures have been developed to achieve ideal performance under different conditions. Due to the special anisotropic property, AMR materials are applied in designing memory sensors and angle sensors [8,9,21]. However, the MR of AMR materials is relatively low (2.5–5%) [22]. Currently, multilayer systems with GMR or TMR effects are widely employed in commercial applications [10–12]. In recent years, emerging nanotechnology has offered various options for constructing ideal MR materials/structures. Instead of the bulk layer, the granular MR system was developed with pressed small granules of magnetic materials. Granular MR systems are designed to reduce the complexity and improve the efficiency of the preparation [23–25].

Due to its unique physical/chemical properties, graphene has soon attracted the attention of researchers [26]. Multilayered graphene, graphene foams, and hybrid graphene nanocomposites have been introduced in the development of MR materials/structures [27–29]. Layered graphene MR systems are constructed by introducing disorders into monolayer/multilayer graphene or combining graphene layers in multilayer devices [30–35].

Graphene foams (GF) are three-dimensional arranged graphene structures with good bio-compatibility and MR property [36–42]. Hybrid graphene nanocomposites with MR are constructed with graphene and reduced graphene oxide (rGO) [29,43–50].

2.1. GMR and TMR Multilayer Systems

The multilayer configuration was adopted in the production of MR sensors since the discovery of giant magnetoresistance (GMR) and tunneling magnetoresistance (TMR). The GMR effect was observed in the Fe/Cr multilayer system, and the TMR effect was discovered in Fe/Ge/Co multilayer system under low temperature (4.2 K) [2,3,51]. As mentioned previously, these multilayer systems consist of ferromagnetic material layers and non-magnetic material layers (GMR) or insulator layers (TMR). Two different configurations (Figure 4) were involved in the fabrication of multilayer systems: current in plane (CIP) and current perpendicular to plane (CPP) [4]. In the CIP configuration, the electrodes are placed on the side of the multilayer with the current flowing along with the multilayer system. The current flows perpendicular to the multilayer system in the CPP configuration, which achieves a higher MR value in contrast with the CIP configuration [52,53]. In multilayer systems, the magnitude of the MR is related to various factors such as layer thickness, number of layer repetitions, layer crystallinity, interface roughness, and band/lattice matching between layers [54].
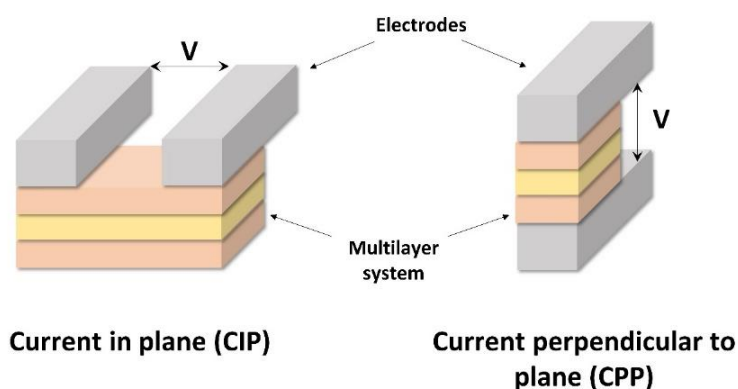

Figure 4. Schematic diagram of current in plane (CIP) configuration and current perpendicular to plane (CPP) configuration.

Accurate control of the layer thickness is crucial for the MR values. Various preparation processes have been involved in the construction of multilayer systems including electron beam evaporation, magnetron sputtering, cathodic arc deposition, molecular beam epitaxy (MBE), pulsed laser deposition (PLD), and chemical vapor deposition (CVD) [55–61]. These techniques provide precise control on the layer thickness and layer repetitions. However, most of these techniques required prolonged/complicated preparation processes and specific equipment/instruments, which leads to increasing economic costs and time costs for production.

Ferromagnetic metals (such as Fe, Co, and Ni) are involved in the fabrication of the ferromagnetic layer in multilayer systems. Meanwhile, non-magnetic layers (Cu, Cr, Ag, Au, Ru, etc.) are applied in the construction of multilayer systems [62]. Alloys such as FeCo and FeNi are adopted in the production of both GMR and TMR multilayer systems due to their strong spin-dependent scattering properties [63,64]. FeCo possesses unique properties such as high saturation magnetization, high curie temperature, and good strength, which are ideal for constructing multilayer systems [65].

The GMR multilayer systems normally consist of ferromagnetic layers with 4~6 nm thickness and 35 nm non-magnetic conductive spacer layer. The GMR and TMR multilayers exhibit good compatibility for integrating with electronic circuits (Figure 5) [66,67]. GMR and some TMR multilayer systems display inadequate MR under the low magnetic field and room temperature. In addition, their applications are hindered by the limited

working range (especially for TMR multilayer systems) and complicated fabrication processes, which require further investigation to overcome current challenges [67].
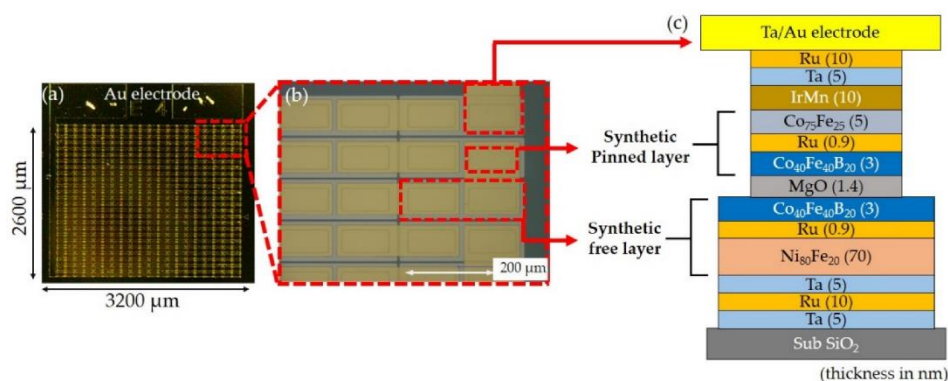

Figure 5. (**a**,**b**) Microscopy of TMR multilayer system consists of 500 MTJs. (**c**) Schematic diagram of TMR multilayer system. Adapted from [67]. Figure Copyright © 2018 MDPI Publishing, Open Access.

2.2. Granular MR Systems

Various methods have been developed to increase the sensitivity of the conventional GMR and TMR multilayer systems. One route is to maximize the layer numbers of the multilayer system. Although it is possible to achieve this architecture via the physical/chemical deposition processes mentioned previously, this route significantly increases the complexity and decreases the efficiency of the production process. The granular MR systems are developed to replace the multilayer configuration, which can increase the sensitivity and reduce the potential economic costs and time costs.

The small grains are pressed together to construct the granular MR system in the first geometry [25]. Another geometry is constructed by embedding the magnetic particles in the non-magnetic matrix (conducting or insulating) [23,24]. The hypothesis suggests that these geometries can improve the magnitude of the MR since every boundary between the granular particles can become a spin-selecting junction [25]. In contrast with the conventional multilayer systems, granular MR systems reduce the investment in instruments and the complexity of the production process. Granular MR systems suffered from non-uniform distributions and poor grain boundaries in the early stages. Chemically/physically prepared nanoparticles have been applied to construct the granular MR systems since emerging nanotechnology provides uniformly dispersed nanoparticles.

Similar to the multilayer systems, nanoparticles containing Fe and Co are employed in the granular MR systems. Chemically synthesized Fe_3O_4 nanoparticles are adopted in constructing granular MR systems because of their accessibility, stability, and large magnetization. The Fe_3O_4 granular MR systems achieved -1.6% and -1.2% of resistance change at 5 kOe for thin film and pressed powder [68]. Various granular MR systems were developed based on core-shell structures of Fe_3O_4 including $Fe_3O_4@SiO_2$, $Fe_3O_4@ZnS$, $Fe_3O_4@ZrO_2$ and $MgO@Fe_3O_4$ [25,69–71]. These granular systems achieved a large linear working range (~2 T) and relatively large negative MR responses (-4%~-8%). However, most of them require low temperatures to obtain satisfactory MR values.

In the meantime, Co is widely applied in constructing granular MR systems. The investigations were performed on Co-Cu, Co-Ag, Co-Ni, and ZnO/ZnO-Co granular MR systems [72–74]. It should be noted that electrodeposition is applied in producing Co-based granular MR systems, which may slightly increase the cost of specific instruments in the preparation. In addition, the chemically synthesized $CoFe_2O_4$ nanoparticles exhibited a large negative MR (-18%~-19%), which was obtained under a high magnetic field (70 kOe) [25].

Another geometry of granular MR systems is based on embedding nanoparticles in the non-magnetic matrix (Figure 6) [75]. Fe nanoparticles were deposited on the SiO_2 matrix with the ion beam, which achieved a positive MR at 40% under a large magnetic field

(80 kOe) and room temperature [76]. Meanwhile, FeCo exhibits good compatibility with the granular MR system that consists of magnetic nanoparticles and the non-magnetic matrix. FeCo processes high saturation magnetization and strong spin-dependent scattering properties, which are favoured in MR materials [77–79].
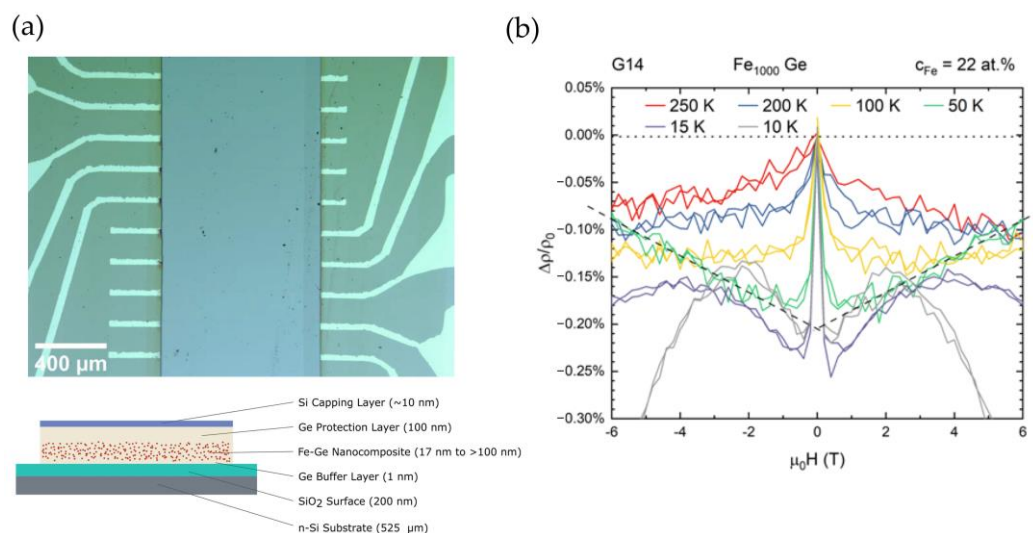
(a) (b)

Figure 6. (**a**) Optical micrograph and schematic diagram of granular MR systems based on Fe nanoparticles in Ge matrix. (**b**) MR of Fe-Ge at different temperatures. Adapted from [75]. Figure Copyright © 2020 MDPI Publishing, Open Access.

FeCo granules/particles have been embedded in Si-N, SiO_2, Al_2O_3, Cu, and carbon matrix by magnetron sputtering technique [77,80–83]. In these studies, FeCo granular systems achieved the MR up to 30% at room temperature. However, the high magnetic field (50 kOe) is the prerequisite for FeCo granular systems to achieve large MR at ambient temperature. Therefore, although granular MR systems can reduce the cost and complexity in producing MR sensors with enhanced sensitivity, the granular systems still display inadequate MR under the low magnetic field ($\leq$10 kOe). In some cases, granular MR systems may require special conditions (i.e., low temperatures, large magnetic fields, etc.) to achieve proper performances.

2.3. Graphene-Based MR Systems

2.3.1. Layered Graphene MR Systems

The discovery of graphene provided a powerful tool for developing MR materials as graphene possesses unique physical and chemical properties [84–87]. Large MR has been observed on MR systems based on monolayer graphene, bilayer graphene, and multilayer graphene (Figure 7) at room temperature or extremely low temperatures (1.9 K) [85,88–92]. The results indicate the feasibility to design MR sensors with layered graphene systems, although specific substrates/preparation techniques are required in most circumstances.

Various methods were developed to enhance the MR of layered graphene systems. Normally, two different routes are applied. The first method relies on introducing disorder into the graphene layers. This method employs the monolayer or multilayer graphene produced by mechanical exfoliation or chemical vapor deposition (CVD) [30,31]. The disorders are introduced by Ga^+ ion irradiation or nitrogen doping [30,31]. The origin of the MR improvements is attributed to the increasing diffuse scattering at crystallite boundaries after the increase of disorders [30,31]. Although this process can improve the performance of layered graphene systems, it requires specific substrate and instrument, which leads to the increase in complexity and investment of the preparation process.
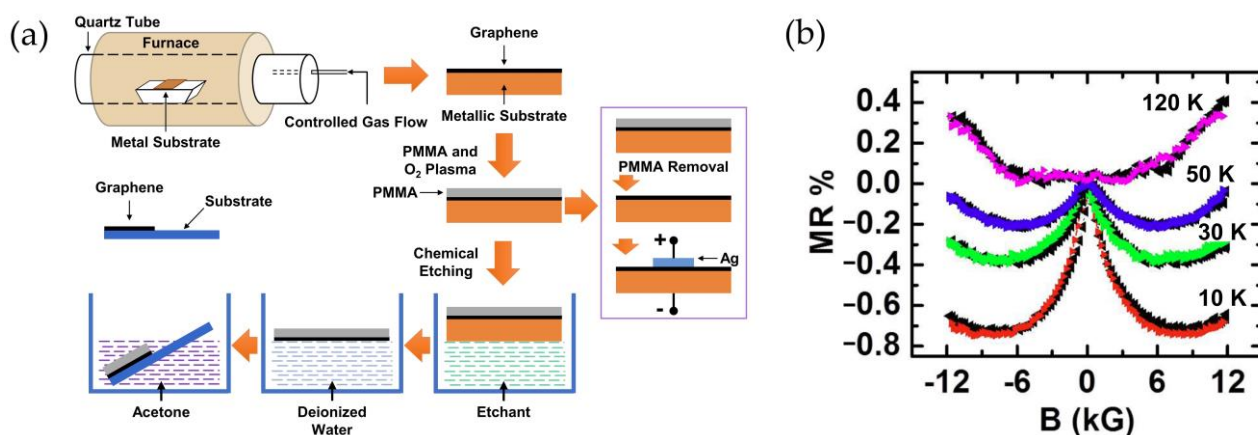
Figure 7. (**a**) Schematic diagram of the fabrication process of multilayer graphene/metal catalyst heterojunction. (**b**) MR of the response of multilayer graphene on Cu substrate. Adapted from [88]. Figure Copyright © 2013 MDPI Publishing, Open Access.

The second method incorporates graphene layers into the multilayer systems. This method combines graphene layers with the other layered materials including using graphene as the inset layer for the multilayer systems or combining graphene with other two-dimensional materials [32–35]. Although some studies achieved significant improvement of MR performance for layered graphene systems, the issues can't be ignored regarding the requirements on specific instruments for producing mono/multilayer graphene and other layered materials.

The layered graphene system is one of the promising materials for developing future MR sensors. However, it is noted that preparing layered graphene systems require specific substrates/circuits and instruments (for precise control of layer number), which increases the cost and complexity of production processes. This hinders the further applications of layered graphene MR systems. Extreme conditions are required to achieve proper MR performances (such as low temperatures). Although various methods were developed to improve the performance of layered graphene systems at room temperature, these methods still rely on specific instruments, which result in prolong processes and low cost-efficiency. Moreover, some layered graphene systems display relatively small MR at the low magnetic field ($\leq$10 kOe), and higher magnetic fields are required to obtain large MR values in most circumstances.

2.3.2. Graphene Foam MR Systems

Graphene foam (GF) attracts the interest of researchers as it provides a solution to transfer two-dimensional material into a three-dimensional architecture. The advantages of graphene foams include biocompatibility, the combination of intrinsic properties of graphene, pore size adjustability, three-dimensional morphology, and potential for mass production [36–39]. Currently, graphene foams have been applied in designing gas sensors, lithium-ion batteries, and supercapacitors [36,93,94]. In addition, graphene foam can also be applied in the production of shapable electronic devices, although it suffers from the problems such as non-flexible structure and unstable mechanical strength.

Recently, researchers discovered interesting magneto-transport properties of graphene foams since three-dimensional graphene foams exhibit different morphology in contrast with two-dimensional graphene [42]. The magneto-transport properties are related to the size of graphene sheets, connections between graphene sheets, the edge boundaries of graphene sheets, and the layer number of graphene sheets in the graphene foams [95–99]. The trajectories of charge carriers are affected by the morphology of graphene in graphene foams under the presence of external magnetic fields [42]. Graphene foams produced by CVD exhibited large MR (80~90%) under the high magnetic field (>50 kOe) and room temperature [41,42,100].

The disorder and inhomogeneity are considered as the crucial factors for MR in graphene foams [100]. Two major routes are applied to further improve the performance of graphene foam MR systems. The first route is to introduce disorder to graphene foam. On the other hand, the second route is to incorporate other nanostructures/nanomaterials with graphene foam. Graphene foams were combined with polydimethylsiloxane (PDMS), poly(methyl methacrylate) (PMMA), and Cu_2ZnSnS_4 nanocrystals to enhance the MR performances or achieve tunable MR [40–42]. In another approach, the inductively coupled plasma system was applied to perform the fluorination of graphene foams for introducing disorders [101].

Currently, graphene foams have exhibited potentials in developing future MR sensors. However, graphene foams require complicated preparation processes that rely on specific equipment for producing graphene foams and introducing disorders. Meanwhile, graphene foams display inadequate MR under low magnetic fields (≤ 10 kOe), and most of the results indicate that graphene foams exhibit large MR under the high magnetic field (≥ 50 kOe). In addition, extreme temperatures (~5 K) are required in some circumstances to obtain satisfactory MR values for graphene foams. Therefore, further investigations could focus on enhancing the MR performance and reducing the complexity of production processes. This would undoubtedly boost the applications of graphene foams for producing future MR sensors.

2.3.3. Hybrid Graphene Nanocomposites MR Systems

Graphene offers unique features such as high carrier mobility, high thermal conductivity, and a large surface-to-volume ratio [102]. The large surface area of graphene allows modifications for different applications (such as polymers, biomolecules, and nanoparticles) [103–105]. The nanoparticles modified graphene has been extensively investigated for various applications including biological medicine, biosensing, gas sensing, catalysis, microwave absorption, and energy storage [106–111]. Hybrid graphene nanocomposites provide outstanding outputs and promising properties in these areas. Therefore, it is possible to applied heterostructures based on hybrid graphene nanocomposites in the fabrication of MR sensors.

Two different routes are adopted to achieve large MR values for hybrid graphene nanocomposites. In the first route, nanoparticles/adatoms clusters are decorated on the surface of CVD/mechanical exfoliation prepared graphene layers by thermal evaporation or electron beam deposition [43–47]. Both positive and negative MR were obtained in this route. Some studies suggested that relatively large MR could be achieved at low magnetic fields (−9% at ~7 kOe). However, this negative MR was reached at an extremely low temperature (10 K), and the MR deteriorated significantly to −3% as the temperature slightly increased to 50 K. Moreover, the physical deposition processes need specific preparation techniques. Specific substrates are required by CVD/mechanical exfoliation-produced graphene. These drawbacks increase the time and equipment investments of the production process, which hinders the possible applications in the future.

Reduced graphene oxide (rGO) was employed by another route to decrease the equipment/time investments. rGO is facile to produce, and it is favourable for mass production [112]. Meanwhile, rGO is an appropriate substrate for nanoparticles due to the large surface area and functional groups on its surface. Therefore, it is possible to modify nanoparticles on the surface of rGO for developing MR materials. The rGO hybrid nanocomposites can significantly decrease the requirements on specific instruments in the preparation process and reduce the complexity of the production process, which is promising for the mass production of future MR sensors. Relatively large MR can be achieved by rGO hybrid nanocomposites [29,48–50]. However, few attempts were made to develop ideal MR sensors based on rGO hybrid nanocomposites. Currently, rGO hybrid nanocomposites display inadequate MR under the low magnetic field (≤ 10 kOe) and room temperature, which is not suitable for future applications.

3. Applications of Magnetoresistance Sensors

The study of William Thomson set the cornerstone for the future developments of MR sensors [1]. However, few research attempts were put into the investigations of MR due to the small magnitude of the MR effect (less than 2%) [113]. The situation was changed when Grünberg and Fert discovered the GMR in 1988. In the meantime, the demands for magnetic sensors raised due to the surge of magnetic data storage systems since the early 70s. This led to a significant boost of studies on MR sensors [2,3]. In 1990, the GMR multilayer system was successfully prepared by IBM Almaden Research Center with high-vacuum DC magnetron sputtering. This result reveals the possibility to produce sensitive MR sensors for improving the storage capacity of magnetic storage devices [114]. After IBM introduced the first GMR reading head in HDD, more and more studies have focused on developing MR sensors for different applications [115].

MR sensors have been employed in different applications including biophysics and the automotive industry since the first commercial GMR sensor came to the market in 1994 [12]. Currently, giant magnetoresistance (GMR) and tunneling magnetoresistance (TMR) have been widely applied in commercial applications [10–12]. Anisotropic magnetoresistance (AMR) has been applied in position sensing due to its anisotropic nature [8,9]. The major applications of MR sensors include magnetic storage (recording), position sensing, current sensing, non-destructive monitoring, and biomedical sensing systems [116–122]. MR sensors have also been applied in producing antilock brakes, magnetocardiography, and galvanic isolators [123–129]. The total value of the magnetic sensor market is expected to exceed 2.0 billion US dollars in 2022 due to the brooming of the modern electronic industry [130]. As shown in Figure 8, the number of the published papers on MR sensors has increased since 1995, which indicates the growing scientific interest in this topic.
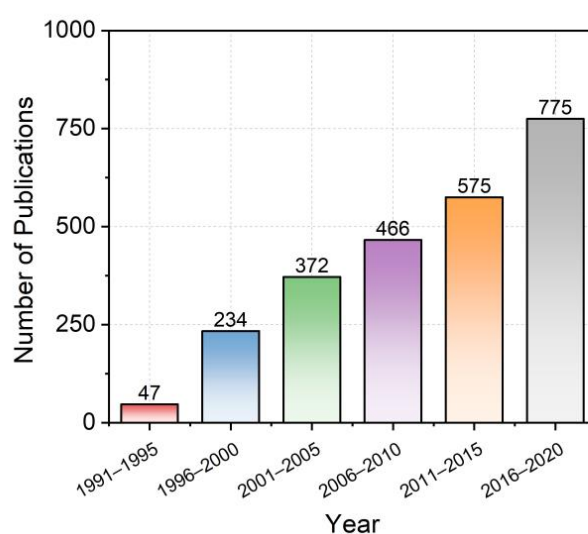

Figure 8. The number of publications on MR sensors from 1991 to 2020. The data were obtained from the Web of Science core collection with the keyword "magnetoresistance sensor".

3.1. MR Sensors in Magnetic Storage

The anisotropic magnetoresistance (AMR) sensor was utilized as the reading head in hard disk drives (HDDs) by IBM since the 1990s [22]. Later, the reading heads were designed on GMR and TMR sensors, which led to the rapid development of the HDDs' storage capacity. The first HDD, IBM 350, can store 4.4 MB of data with 2 kb/in^2 areal density [131]. In contrast with IBM 350, current HDDs can be 2×10^6 higher in data storage (10 TB) with the areal density reaching 1 Tb/in^2. Meanwhile, the average retail price of HDDs has decreased dramatically as a result of the huge advance in the areal density of data [22]. The cost of storing digital data is close to \$$10^6$ per GB in IBM 350, and it is \$0.01 per GB for modern HDDs.

The emergence of the MR sensor has introduced the AMR reading head, GMR reading head, and TMR reading head in 1991, 1997, and 2006, respectively [132–134]. A significant improvement of CGR (from 25% per year to 60% per year) occurred in 1991 as IBM introduced the MR reading head in HDDs. The CGR was further improved to 100% after introducing the GMR reading head. Although the AMR reading head significantly boosts the development of the HDDs, further applications are hindered by the low MR performance and difficulties in reducing the size. Therefore, GMR and TMR sensors have become the mainstream MR reading heads applied in HDDs.

As shown in Figure 9, the read-write head of HDD consists of a traditional coil-structure writing head and a GMR or TMR reading head. The traditional coil structure writing head is used to adjust the magnetization of data bits. In the meantime, The MR reading head is applied to detect the magnetic field of data bits. The variation of magnetic fields can influence the resistance of the MR reading head. The signals of resistance change will be collected by electronic devices.
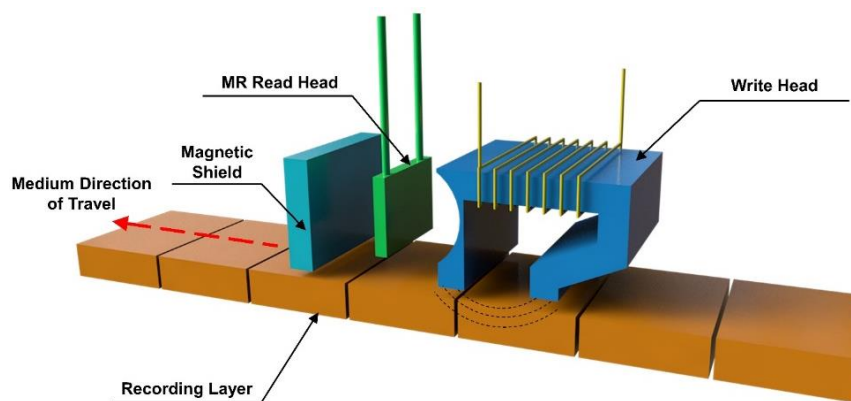

Figure 9. Schematic diagram of the modern read-write head for HDDs. The data bits are displayed in the recording layer.

GMR reading heads are considered as the starting point of the era of modern MR sensors, which increase the MR responses and decrease the device dimensions [4]. The TMR effect exhibits a large MR within a small range of the magnetic field, which is appropriate for sensing the data bits since the outputs are "0" and "1". It is challenging to further decrease the size of TMR reading heads due to the obstacles for reducing the thickness of the insulator layer. Studies are performed to seek MR materials that can replace the current TMR sensors [134].

Another important application is magnetic random-access memory (MRAM). MRAM requires less static power consumption since the data can be stored by magnetization [135,136]. Random access memory (RAM) is an important component of modern electronic devices. Nowadays, electronic devices mainly employ dynamic random-access memory (DRAM) in production, which bases on semiconductor technologies. The key feature of DRAM is volatile property. DRAM may lose all the data after power-off as it is constructed on the circuits with capacitors. Currently, the semiconductor-based DRAMs are facing difficulties to keep the significant growth rate for the storage capacity due to the increased power consumption, which is triggered by the charge leakage problem in reducing the dimension of DRAMs. Therefore, non-volatile memories attract the interest of researchers due to their low power consumption.

MRAM is one of the candidates with features including non-volatility, unlimited read and writes cycles, and high-speed operation [137]. Magnetic tunnel junction (MTJ) is the major component for data storage in MRAMs. As shown in Figure 10, the MTJ displays low resistance under the parallel magnetization directions of the fixed layer and the free layer. It exports a high resistance output at the anti-parallel state. The data stability of MRAMs is not influenced by the measurement and power cut-off in contrast with DRAMs. Although

MRAMs exhibit better scalability and relatively low writing current compared with other RAMs, the reliability issues of MRAMs can't be ignored, which can be caused by oxide barrier breakdown and barrier thickness variability [138]. Therefore, further investigations are required for MRAMs to meet the demands of ideal RAM in the future [139].
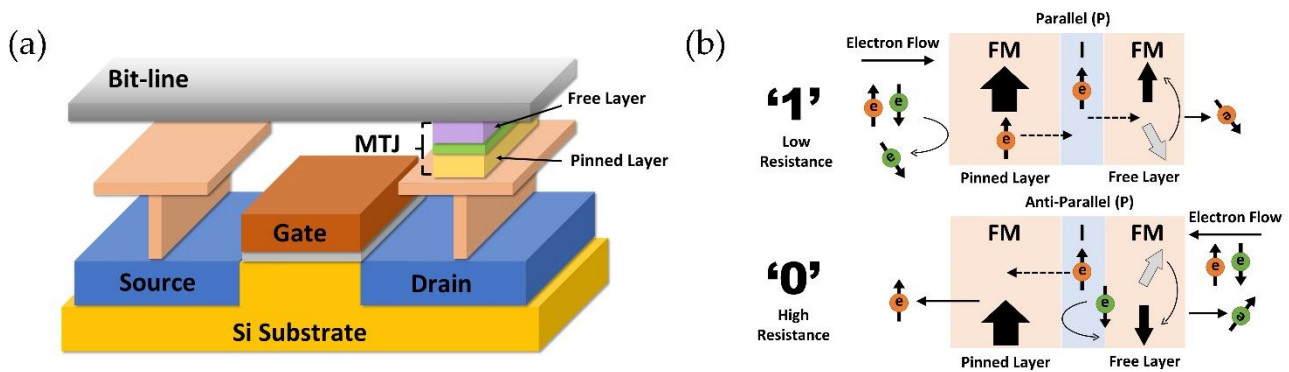

Figure 10. Schematic diagram of (**a**) MRAM cell and (**b**) TMR multilayer system at parallel and anti-parallel magnetizations.

3.2. MR Sensors in Position Sensing, Current Sensing, and Non-Destructive Monitoring

Magnetic sensors (including MR sensors) have been widely applied in position sensing, current sensing, and non-destructive monitoring (Figure 11) [140–150]. In these applications, magnetic sensors are applied to detect the magnetic fields generated by the targets. The magnetic signals are subsequently transferred to other outputs (such as voltage changes, current changes, and resistance changes). Magnetic displacement sensors have been broadly applied in position sensing. Magnetic sensors are cost-effective, stable, and contact-free compared with other sensors in this field [151,152]. Magnetic field sensors are crucial parts of magnetic position sensing systems. In position sensing, two major categories of magnetic sensors are Hall effect sensors and MR sensors [153–155]. MR sensors are more suitable for position sensing because of the high sensitivity, low power consumption, and larger detection range in contrast with traditional Hall effect sensors.
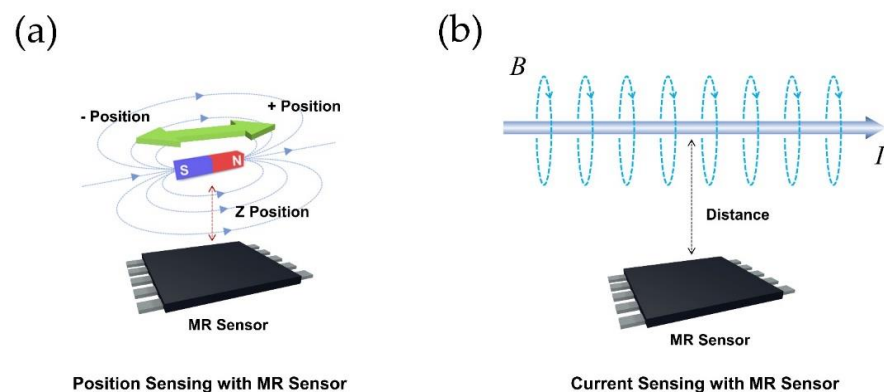
Figure 11. Schematic diagram of (**a**) position sensing and (**b**) current sensing with MR sensors.

Sensor arrays are designed and constructed with GMR/TMR multilayer system to achieve two-dimensional and three-dimensional detections [156–158]. The close-packed MR sensor array was built to dynamically detect magnetic microparticles with high precision. This sensor array can detect the magnetic field in the range of ±500 Oe due to the limitation on the detection range of TMR. Despite the limited working range, it still set a good example to detect travelling particles with the MR sensor array. Another route integrates multiple GMR/TMR sensors with specifically designed circuits. The output signals are analyzed with computer-based driving/detection systems to obtain the magnetic field components at x-, y-, and z-axis.

The detection target is the magnetic field generated by the electrical current in (electrical) current sensing and non-destructive monitoring (as called non-destructive testing (NDT)). GMR/TMR sensors are applied in constructing magnetic electrical current sensing systems. The MR current sensing system is employed in differentiating currents, switching regulators, wattmeters, independent voltage/current measurement, and voltage/current measurement multiplying. Meanwhile, MR sensors are adopted in current sensing devices for integrated circuits (IC) monitoring (such as miliwattmeters and electrical isolators) [95]. The smart grid is another important field for MR sensors in electrical current sensing. Special designed MR sensors are applied since various types of currents need to be measured in the smart grid [159].

Non-destructive monitoring (or non-destructive testing) is a crucial tool to inspect the defects in metallic materials. Non-destructive monitoring is a quality control tool that is applied to inspect the cracks and defects in large structures (such as oil pipes, gas tanks, and aircraft frames) in the industry (also called non-destructive testing (NDT) or non-destructive evaluation and monitoring (NDEM)). This method aims to detect the subsurface mechanical and chemical damages without causing destruction [160,161]. Two different sensing routes are adopted for non-destructive monitoring with magnetic field sensors: magnetic flux leakage testing and eddy current testing. The first route utilizes the breaks of magnetic field lines caused by the surface breaking [162]. Eddy current testing is a more commonly applied testing route for probes equipped with MR sensors [163]. Eddy current is introduced by the external magnetic field source. The inspection is performed to detect both surface and subsurface defects. Compared with the conventional probes, the GMR and TMR sensors exhibit significant increases in efficiency during the inspection of eddy currents due to improvements in the sensitivity of the probe. The accuracy can be increased to 98.2% and 99.4% for reading excitation magnetic fields in the detection of subsurface defects (DC excitation and AC excitation). Therefore, MR sensors are promising for the eddy current testing, and they can certainly benefit the future industrial applications of non-destructive monitoring.

3.3. MR Sensors in Biomedical Sensing Systems

The development of biomedical sensing platforms has been boosted in the past decade thanks to nanobiotechnology. The MR sensor-based biomedical sensing platforms have attracted the interest of researchers since they are sensitive, compact, user-friendly, and cost-effective. MR biosensors experience low background noise in contrast to other biosensors (optical, plasmonic, and electrochemical) since most of the biological environments are nonmagnetic. Therefore, the target's medium triggers limited negative effects, which leads to the reliable and high-precision detection of magnetic labels [164].

In the typical sensing process, the functionalized magnetic nanoparticles (MNPs) are adopted as the magnetic labels. The sensing process is performed by detecting the magnetic fields of MNPs with MR sensors. Variations of the magnetic field's intensity are related to quantity differences of MNPs. Magnetic signals are transferred to other processable signals such as resistance change or current change [165]. Compared with other nanomaterials, the advantages of MNPs include high stability, less operating difficulty, and a high signal-to-noise ratio.

The capture probes are firstly immobilized on the surface of MR sensors [166]. The analytes attached with MNPs can be grubbed by capture probes on the surface of MR sensors for sequential magnetic field sensing [167]. The MR sensor-based biological sensing platforms have attracted the interest of researchers since the first GMR biosensor array was developed in 1998 [168]. Currently, MR biosensors are applied in three major categories of biomedical applications: biomedical diagnosis, food safety, and environmental monitoring [127,169–176].

MR sensors-based biomedical sensing platforms are suitable for diagnosis applications. The precise and robust diagnosis technique is decisive for treating patients and restricting the spread of the diseases [171]. Various proof-of-concept MR biosensors were designed

for diagnosis even in the early stages of MR devices' development [177,178]. GMR and TMR sensors were applied in the direct detection of proteins and antigens such as endoglin, pregnancy-associated plasma protein-A (PAPP-A), proprotein convertase subtilisin/kexin type 9 (PCSK9), and suppression of tumorigenicity 2 (ST2) [179,180]. In these biosensing platforms, the nano-sized MR sensors were applied for real-time monitoring and quantitative detection of the targets in the human serum, which were used to construct the array of GMR sensors. The limit of detection (LOD) reached 40 pg/mL in this process.

Other important topics of biosensing include early detection and diagnosis of cancers and the monitoring of tumors for therapeutic goals. These applications demand enhanced sensitivity and specificity for cancer diagnosis. The GMR biosensing platforms successfully detected cancer antigens including interleukin 6 (IL6), human epididymis protein 4 (HE4), and cancer antigen 125 (CA125 II). GMR biosensors achieved the LODs at the level of 7.4 pg/mL, 3.7 U/mL, and 7.4 pg/mL in these applications [181]. Meanwhile, the GMR biosensing platform was combined with microfluidics for simultaneous detection of 12 tumor markers including human chorionic gonadotropin (free β-hCG) and alpha-fetoprotein (AFP) [182]. This system achieved multi-analyte detection with the LOD at ng/mL level, which can significantly reduce the complexity of the conventional test process.

MR biosensing platforms successfully detected influenza viruses including H1N1 and H3N2v in solution and nasal swab [7,183]. A portable device was developed to meet the requirements of point-of-care (POC) applications. The LODs for H1N1 and H3N2v are both 250 $TCID_{50}$/mL. Meanwhile, the MR immunoassay achieved LODs at the level of 10 ng/mL and 50 ng/mL for detection of human immunoglobulins G and M (IgG and IgM) [184]. MR biosensors were also applied in detecting hepatitis B virus (HBV), hepatitis E virus (HEV), and human immunodeficiency virus (HIV) [185–187].

The detection of bacteria is another important topic due to the serious consequences of bacterial infections. For example, *Escherichia coli (E. coli)* can trigger diseases such as urinary tract infection (UTI). In the meantime, food safety is another application that requires the detection of bacteria. The pathogenic bacteria in food have become one of the major health and public concerns nowadays. The detection of bacteria with MR biosensors follows a similar mechanism with the previously discussed MR biosensing platforms. The TMR sensor array has been applied in the detection of *E. coli* O157:H7 with a LOD at 10^2 CFU/mL [188]. Meanwhile, microfluidics was employed in the GMR biosensing platform for *E.coli* detection [189]. Moreover, the GMR biosensing platform accomplished the detection of the DNA of *salmonellae* [190].

In the meantime, the detections of mycotoxins and allergens are important for food safety. The GMR sensor array was applied in the detection of various mycotoxins such as aflatoxins B1 and zearalenone with a LOD at 50 pg/mL. This array achieved simultaneous detection for various mycotoxins [191]. MR biosensing platforms are capable of detecting major peanut allergens ara h1, ara h2, and gliadin, which can trigger a serious response. The LODs of these allergens can reach 7.0 ng/mL, 0.2 ng/mL, and 1.5 ng/mL [192]. Although MR biosensing platforms exhibit low LODs, the 96 well ELISAs still display a higher sensitivity in terms of the allergens testing. Further studies are required in this area to improve the sensitivity [171].

Environmental monitoring is another major application of MR sensor-based biosensing platforms. This application analyzes the hazardous contents and pollutants in the environment as they can accumulate in the human body through the food chain. The GMR biosensing platform was modified with thymine-thymine (TT) molecules, which achieved precise detection of mercury ions (Hg^{2+}) in the natural environment [193]. The LOD is at the level of 10 nM for buffer and natural water. In another study, the ricin toxins were detected by the TMR biosensing platform in polluted water. The TMR biosensing platform completed the quantitative detection of ricin toxins with a LOD at 1 ng/mL [194]. The TMR biosensing platform experiences minimum interferences from the other contents and environmental factors. These results indicate the possibility for the MR biosensing platform to finish detections of hazard contents in other complex samples such as soil, food, and blood.

Further improvements are required for MR biosensing platforms to meet the demands of clinical implements. Meanwhile, MR biosensing platforms display superiorities such as simultaneous detection, user-friendly procedures, and simple integration with electronic devices. MR biosensing platform is a promising candidate for the development of ideal next-generation biosensing systems. Currently, MR biosensing platforms experience difficulties in the magnitude of MR (especially for low magnetic fields), sensing range, and investments for commercially accessible MR sensors [171]. Moreover, the performance of multilayer systems is inadequate at room temperature [171]. Although the TMR multilayer system could display a large MR, the limited working range can't be ignored. GMR/TMR multilayer systems could be expensive compared with traditional testing approaches due to the complicated preparation processes. The price of MR sensors limits the commercial applications of MR biomedical sensing platforms. Therefore, further investigations are required on developing cost-effective MR sensors with enhanced MR response at low magnetic field/room temperature, which can benefit the future commercial applications of MR biomedical sensing systems.

4. Conclusions

Since the first observation of MR, more and more attempts have been put into the development of ideal MR sensors for various applications. Meanwhile, many studies were performed to extend the application of MR sensors [116–122]. The major applications of MR sensors include magnetic storage, position sensing, current sensing, non-destructive monitoring, and biomedical sensing system. Meanwhile, MR sensors were applied in antilock brakes, magnetocardiography, and galvanic isolators [123–129]. The expansion of the electronic industry leads to the significant growth of commercial magnetic sensors. The total value of the market is expected to surpass 2.0 billion US dollars in 2022 [130].

The sensitivity and efficiency are crucial to commercial MR sensors in terms of improving the performance of the devices. Ideal MR sensors require enhanced MR at low magnetic fields and room temperature, reduced time/equipment cost, and enlarged working range, which can boost the advancement of devices with built-in MR units. In specific, ideal MR materials contribute to improving the storage capacity and decreasing the production cost of magnetic storage devices (such as HDDs and MRAMs). More details can be provided in position sensing, current sensing, and non-destructive monitoring since the sensitivity and cost-efficiency are enhanced for MR sensors. The LOD relies on the performance of MR sensors in magnetic biomedical sensing platforms/systems (especially for ultra-low detections). The improvements of MR sensors can lower the LOD of MR biomedical sensing platforms. Meanwhile, the decrease in production costs can help to improve the accessibility of MR sensor-based point-of-care (POC) testing devices.

Various MR materials have been studied to enhance the performance of MR sensors as shown in Table 1. GMR and TMR multilayer systems have been widely applied in commercial MR sensors [10–12]. However, the drawbacks of multilayer systems can't be ignored including inadequate MR at room temperature and low magnetic fields, limited working range, and complicated preparation process. Many attempts have been made to develop nanoconstructed MR materials such as granular MR materials, layered graphene, graphene foam, and hybrid graphene nanocomposites [40,48,77,85]. However, current MR materials experience difficulties in enhancing the MR at low magnetic fields/room temperature and reducing the complicity of the preparation process. Breakthroughs are expected to improve the performance and reduce the manufacturing cost of devices with built-in MR units, which overcome existing challenges and benefit the future application of MR sensors.

Table 1. Summary of current magnetoresistance (MR) materials.

Type	Advantages	Disadvantages	Ref
AMR materials	Anisotropic properties of AMR materials have advantages in position sensing and navigation (angular and displacement sensing)	The low magnitude of AMR outputs ($\Delta R/R_0 < 2.5\%$) Difficult to reduce the size and hard for miniaturization	[8,9]
Multilayer systems based on GMR and TMR	GMR/TMR multilayer systems exhibit high sensitivity for low magnetic fields GMR/TMR multilayer systems can be integrated with the electronic circuit easily	Multilayer structures require complicated fabrication processes and specific equipment due to the strict limitations of layer thickness (increasing cost on equipment and extending the fabrication process lead to expensive products) GMR/TMR multilayer systems exhibit limited resistance variation range (working range, especially for TMR) and relatively low MR at room temperature (mostly for GMR)	[52–61,65–67]
Granular MR systems	Granular MR systems bring simplified fabrication procedures and reduced investments in instruments Relatively large MR at room temperature can be achieved by some specific designed granular MR systems	Magnetic field ≥ 50 kOe is the prerequisite to achieve large MR at ambient temperature (relatively small resistance change for low magnetic fields at room temperature) Some granular MR systems require extremely low temperatures for large MR Although granular MR systems can reduce the complexity of the fabrication process, the dependence on specific fabrication techniques (such as magnetron sputtering) remains	[23–25,68–74]
Layered graphene MR systems	Layered graphene MR systems exhibit large MR value and potential to be applied on fabricating next-generation spintronics based on layered graphene	Most layered graphene MR systems require extremely low temperatures to achieve large MR Special designed substrates/circuits are required Precise control of layer number and positions is challenging Special fabrication techniques are required for preparing layered graphene, which further increases the production costs and the complexity	[30–35,85,89–91]
Graphene foam MR systems	Graphene foam MR systems display relatively large MR at room temperature and offer unique 3-D structures for potential applications	Large magnetic fields (≥ 50 kOe) are required for graphene foams to reach considerable MR (the magnitude of resistance change shrinks rapidly as the magnetic field reduce to the level of 10 kOe) Graphene foams require complicated fabrication processes (such as CVD) and specific defects-introducing instruments	[41,42,100,101]

Table 1. *Cont.*

Type		Advantages	Disadvantages	Ref
Hybrid graphene nanocomposites	Based on CVD/mechanical exfoliation produced graphene	Relatively large values were achieved for both positive and negative MR Future applications in fabricating graphene-based circuits	Special designed substrate/circuits are required for CVD/mechanical exfoliation produced graphene leads to complicated fabrication processes with more investments and time costs Exhibiting small magnitude of MR at room temperature	[43–47]
	Based on reduced graphene oxide (rGO)	rGO and rGO hybrid nanocomposites can be both obtained with facile preparation processes leads to lesser requirements on special equipment Reduced investments in instruments and simplified production process (cost-effective and friendly for mass production) Large MR was achieved by the rGO hybrid nanocomposites	Current results of rGO hybrid nanocomposites show relatively small MR at the low magnetic field (<10 kOe) and room temperature Few investigations have been performed to develop and improve the MR of rGO hybrid nanocomposites	[29,48–50]

References

1. Thomson, W., XIX. On the electro-dynamic qualities of metals:—Effects of magnetization on the electric conductivity of nickel and of iron. *Proc. R. Soc. London* **1857**, *8*, 546–550.
2. Baibich, M.N.; Broto, J.M.; Fert, A.; Van Dau, F.N.; Petroff, F.; Etienne, P.; Creuzet, G.; Friederich, A.; Chazelas, J. Giant Magnetoresistance of (001)Fe/(001)Cr Magnetic Superlattices. *Phys. Rev. Lett.* **1988**, *61*, 2472–2475. [CrossRef] [PubMed]
3. Binasch, G.; Grünberg, P.; Saurenbach, F.; Zinn, W. Enhanced magnetoresistance in layered magnetic structures with antiferromagnetic interlayer exchange. *Phys. Rev. B* **1989**, *39*, 4828–4830. [CrossRef] [PubMed]
4. Chappert, C.; Fert, A.; Van Dau, F.N. The emergence of spin electronics in data storage. *Nat. Mater.* **2007**, *6*, 813. [CrossRef] [PubMed]
5. Kartik, V.; Sebastian, A.; Tuma, T.; Pantazi, A.; Pozidis, H.; Sahoo, D.R. High-bandwidth nanopositioner with magnetoresistance based position sensing. *Mechatronics* **2012**, *22*, 295–301. [CrossRef]
6. Hamia, R.; Cordier, C.; Dolabdjian, C. Eddy-current non-destructive testing system for the determination of crack orientation. *NDT E Int.* **2014**, *61*, 24–28. [CrossRef]
7. Krishna, V.D.; Wu, K.; Perez, A.M.; Wang, J.-P. Giant Magnetoresistance-based Biosensor for Detection of Influenza A Virus. *Front. Microbiol.* **2016**, *7*, 400. [CrossRef]
8. Demirci, E. Magnetic and Magnetotransport Properties of Memory Sensors Based on Anisotropic Magnetoresistance. *J. Supercond. Novel Magn.* **2020**, *33*, 3835–3840. [CrossRef]
9. Sreevidya, P.V.; Borole, U.P.; Kadam, R.; Khan, J.; Barshilia, H.C.; Chowdhury, P. A novel AMR based angle sensor with reduced harmonic errors for automotive applications. *Sens. Actuators A* **2021**, *324*, 112573.
10. Ouyang, Y.; Wang, Z.; Zhao, G.; Hu, J.; Ji, S.; He, J.; Wang, S.X. Current sensors based on GMR effect for smart grid applications. *Sens. Actuators A* **2019**, *294*, 8–16. [CrossRef]
11. Schnitzspan, L.; Cramer, J.; Kubik, J.; Tarequzzaman, M.; Jakob, G.; Kläui, M. Impact of Annealing Temperature on Tunneling Magnetoresistance Multilayer Stacks. *IEEE Magn. Lett.* **2020**, *11*, 1–5. [CrossRef]
12. Tumanski, S. *Thin film magnetoresistive sensors*; CRC Press: Boca Raton, FL, USA, 2001.
13. Velev, J.; Sabirianov, R.F.; Jaswal, S.S.; Tsymbal, E.Y. Ballistic Anisotropic Magnetoresistance. *Phys. Rev. Lett.* **2005**, *94*, 127203. [CrossRef]
14. Campbell, I.A.; Fert, A. Chapter 9 Transport properties of ferromagnets. In *Handbook of Ferromagnetic Materials*; Elsevier: Amsterdam, The Netherlands, 1982; Volume 3, pp. 747–804.
15. Campbell, I.A.; Fert, A.; Jaoul, O. The spontaneous resistivity anisotropy in Ni-based alloys. *J. Phys. C Solid State Phys.* **1970**, *3*, S95–S101. [CrossRef]
16. Kokado, S.; Tsunoda, M. Anisotropic Magnetoresistance Effect: General Expression of AMR Ratio and Intuitive Explanation for Sign of AMR Ratio. *Adv. Mat. Res.* **2013**, *750–752*, 978–982. [CrossRef]
17. Zahn, P.; Binder, J.; Mertig, I.; Zeller, R.; Dederichs, P.H. Origin of Giant Magnetoresistance: Bulk or Interface Scattering. *Phys. Rev. Lett.* **1998**, *80*, 4309–4312. [CrossRef]
18. Fert, A.; Campbell, I.A. Two-Current Conduction in Nickel. *Phys. Rev. Lett.* **1968**, *21*, 1190–1192. [CrossRef]
19. Inoue, J.; Maekawa, S. Theory of tunneling magnetoresistance in granular magnetic films. *Phys. Rev. B* **1996**, *53*, R11927–R11929. [CrossRef] [PubMed]
20. Zhu, J.-G.; Park, C. Magnetic tunnel junctions. *Mater. Today* **2006**, *9*, 36–45. [CrossRef]
21. Guo, Y.; Deng, Y.; Wang, S.X. Multilayer anisotropic magnetoresistive angle sensor. *Sens. Actuators A Phys.* **2017**, *263*, 159–165. [CrossRef]
22. Fullerton, E.E.; Childress, J.R. Spintronics, Magnetoresistive Heads, and the Emergence of the Digital World. *Proc. IEEE* **2016**, *104*, 1787–1795. [CrossRef]
23. Berkowitz, A.E.; Mitchell, J.R.; Carey, M.J.; Young, A.P.; Zhang, S.; Spada, F.E.; Parker, F.T.; Hutten, A.; Thomas, G. Giant magnetoresistance in heterogeneous Cu-Co alloys. *Phys. Rev. Lett.* **1992**, *68*, 3745–3748. [CrossRef]

24. Xiao, J.Q.; Jiang, J.S.; Chien, C.L. Giant magnetoresistance in nonmultilayer magnetic systems. *Phys. Rev. Lett.* **1992**, *68*, 3749–3752. [CrossRef] [PubMed]

25. Zhou, B.H.; Rinehart, J.D. A Size Threshold for Enhanced Magnetoresistance in Colloidally Prepared $CoFe_2O_4$ Nanoparticle Solids. *ACS Cent. Sci.* **2018**, *4*, 1222–1227. [CrossRef]

26. Novoselov, K.S.; Fal'ko, V.I.; Colombo, L.; Gellert, P.R.; Schwab, M.G.; Kim, K. A roadmap for graphene. *Nature* **2012**, *490*, 192–200. [CrossRef]

27. Chen, J.-J.; Meng, J.; Zhou, Y.-B.; Wu, H.-C.; Bie, Y.-Q.; Liao, Z.-M.; Yu, D.-P. Layer-by-layer assembly of vertically conducting graphene devices. *Nat. Commun.* **2013**, *4*, 1921. [CrossRef]

28. Sagar, R.U.R.; Qazi, H.I.A.; Zeb, M.H.; Stadler, F.J.; Shabbir, B.; Wang, X.; Zhang, M. Tunable sign of magnetoresistance in graphene foam – Ecoflex®composite for wearable magnetoelectronic devices. *Mater. Lett.* **2019**, *253*, 166–170. [CrossRef]

29. Zhu, J.; Luo, Z.; Wu, S.; Haldolaarachchige, N.; Young, D.P.; Wei, S.; Guo, Z. Magnetic graphene nanocomposites: Electron conduction, giant magnetoresistance and tunable negative permittivity. *J. Mater. Chem.* **2012**, *22*, 835–844. [CrossRef]

30. Rein, M.; Richter, N.; Parvez, K.; Feng, X.; Sachdev, H.; Kläui, M.; Müllen, K. Magnetoresistance and Charge Transport in Graphene Governed by Nitrogen Dopants. *ACS Nano* **2015**, *9*, 1360–1366. [CrossRef] [PubMed]

31. Zhou, Y.-B.; Han, B.-H.; Liao, Z.-M.; Wu, H.-C.; Yu, D.-P. From positive to negative magnetoresistance in graphene with increasing disorder. *Appl. Phys. Lett.* **2011**, *98*, 222502. [CrossRef]

32. Gopinadhan, K.; Shin, Y.J.; Jalil, R.; Venkatesan, T.; Geim, A.K.; Neto, A.H.C.; Yang, H. Extremely large magnetoresistance in few-layer graphene/boron–nitride heterostructures. *Nat. Commun.* **2015**, *6*, 8337. [CrossRef]

33. Asshoff, P.U.; Sambricio, J.L.; Rooney, A.P.; Slizovskiy, S.; Mishchenko, A.; Rakowski, A.M.; Hill, E.W.; Geim, A.K.; Haigh, S.J.; Fal'ko, V.I.; et al. Magnetoresistance of vertical Co-graphene-NiFe junctions controlled by charge transfer and proximity-induced spin splitting in graphene. *2D Mater.* **2017**, *4*, 031004. [CrossRef]

34. Huang, H.; Guan, H.; Su, M.; Zhang, X.; Liu, Y.; Liu, C.; Zhang, Z.; Liu, K.; Liao, L.; Tang, N. Gate-tunable linear magnetoresistance in molybdenum disulfide field-effect transistors with graphene insertion layer. *Nano Res.* **2020**, *14*, 1814–1818. [CrossRef]

35. Cobas, E.D.; van 't Erve, O.M.J.; Cheng, S.-F.; Culbertson, J.C.; Jernigan, G.G.; Bussman, K.; Jonker, B.T. Room-Temperature Spin Filtering in Metallic Ferromagnet–Multilayer Graphene–Ferromagnet Junctions. *ACS Nano* **2016**, *10*, 10357–10365. [CrossRef] [PubMed]

36. Sagar, R.U.R.; Mahmood, N.; Stadler, F.J.; Anwar, T.; Navale, S.T.; Shehzad, K.; Du, B. High Capacity Retention Anode Material for Lithium Ion Battery. *Electrochim. Acta* **2016**, *211*, 156–163. [CrossRef]

37. Chen, Z.; Ren, W.; Gao, L.; Liu, B.; Pei, S.; Cheng, H.-M. Three-dimensional flexible and conductive interconnected graphene networks grown by chemical vapour deposition. *Nat. Mater.* **2011**, *10*, 424–428. [CrossRef] [PubMed]

38. Ma, Y.; Chen, Y. Three-dimensional graphene networks: Synthesis, properties and applications. *Natl. Sci. Rev.* **2015**, *2*, 40–53. [CrossRef]

39. Krueger, E.; Chang, A.N.; Brown, D.; Eixenberger, J.; Brown, R.; Rastegar, S.; Yocham, K.M.; Cantley, K.D.; Estrada, D. Graphene Foam as a Three-Dimensional Platform for Myotube Growth. *ACS Biomater. Sci. Eng.* **2016**, *2*, 1234–1241. [CrossRef] [PubMed]

40. Zeb, M.H.; Shabbir, B.; Sagar, R.U.R.; Mahmood, N.; Chen, K.; Qasim, I.; Malik, M.I.; Yu, W.; Hossain, M.M.; Dai, Z.; et al. Superior Magnetoresistance Performance of Hybrid Graphene Foam/Metal Sulfide Nanocrystal Devices. *ACS Appl. Mater. Interfaces* **2019**, *11*, 19397–19403. [CrossRef]

41. Sagar, R.U.R.; Galluzzi, M.; García-Peñas, A.; Bhat, M.A.; Zhang, M.; Stadler, F.J. Large unsaturated room temperature negative magnetoresistance in graphene foam composite for wearable and flexible magnetoelectronics. *Nano Res.* **2019**, *12*, 101–107. [CrossRef]

42. Sagar, R.U.R.; Galluzzi, M.; Wan, C.; Shehzad, K.; Navale, S.T.; Anwar, T.; Mane, R.S.; Piao, H.-G.; Ali, A.; Stadler, F.J. Large, Linear, and Tunable Positive Magnetoresistance of Mechanically Stable Graphene Foam–Toward High-Performance Magnetic Field Sensors. *ACS Appl. Mater. Interfaces* **2017**, *9*, 1891–1898. [CrossRef] [PubMed]

43. Cai, C.-Y.; Chen, J.-H. Electronic transport properties of Co cluster-decorated graphene. *Chin. Phys. B* **2018**, *27*, 067304. [CrossRef]

44. Chandni, U.; Henriksen, E.A.; Eisenstein, J.P. Transport in indium-decorated graphene. *Phys. Rev. B* **2015**, *91*, 245402. [CrossRef]

45. Elias, J.A.; Henriksen, E.A. Electronic transport and scattering times in tungsten-decorated graphene. *Phys. Rev. B* **2017**, *95*, 075405. [CrossRef]

46. Jia, Z.; Zhang, R.; Han, Q.; Yan, Q.; Zhu, R.; Yu, D.; Wu, X. Large tunable linear magnetoresistance in gold nanoparticle decorated graphene. *Appl. Phys. Lett.* **2014**, *105*, 143103. [CrossRef]

47. Wang, Y.; Jaiswal, M.; Lin, M.; Saha, S.; Özyilmaz, B.; Loh, K.P. Electronic Properties of Nanodiamond Decorated Graphene. *ACS Nano* **2012**, *6*, 1018–1025. [CrossRef] [PubMed]

48. Abellán, G.; Prima-García, H.; Coronado, E. Graphene enhances the magnetoresistance of $FeNi_3$ nanoparticles in hierarchical $FeNi_3$–graphene nanocomposites. *J. Mater. Chem. C* **2016**, *4*, 2252–2258. [CrossRef]

49. Majumder, C.; Bhattacharya, S.; Saha, S.K. Anomalous large negative magnetoresistance in transition-metal decorated graphene: Evidence for electron-hole puddles. *Phys. Rev. B* **2019**, *99*, 045408. [CrossRef]

50. Sheykhifard, Z.; Mohseni, S.M.; Tork, B.; Hajiali, M.R.; Jamilpanah, L.; Rahmati, B.; Haddadi, F.; Hamdi, M.; Mohseni, S.M.; Mohammadbeigi, M.; et al. Magnetic graphene/Ni-nano-crystal hybrid for small field magnetoresistive effect synthesized via electrochemical exfoliation/deposition technique. *J. Mater. Sci. Mater. Electron.* **2018**, *29*, 4171–4178. [CrossRef]

51. Julliere, M. Tunneling between ferromagnetic films. *Phys. Lett. A* **1975**, *54*, 225–226. [CrossRef]

52. Valet, T.; Fert, A. Theory of the perpendicular magnetoresistance in magnetic multilayers. *Phys. Rev. B* **1993**, *48*, 7099–7113. [CrossRef]

53. Bass, J.; Pratt, W.P. Current-perpendicular (CPP) magnetoresistance in magnetic metallic multilayers. *J. Magn. Magn. Mater.* **1999**, *200*, 274–289. [CrossRef]

54. Tsymbal, E.Y.; Pettifor, D.G. Perspectives of giant magnetoresistance. In *Solid State Physics*; Ehrenreich, H., Spaepen, F., Eds.; Academic Press: Amsterdam, The Netherlands, 2001; Volume 56, pp. 113–237.

55. Kąc, M.; Morgiel, J.; Polit, A.; Zabila, Y.; Marszałek, M. Atomic scale structure investigations of epitaxial Fe/Cr multilayers. *Appl. Surf. Sci.* **2014**, *305*, 154–159. [CrossRef]

56. Kąc, M.; Polit, A.; Dobrowolska, A.; Zabila, Y.; Krupiński, M.; Marszałek, M. Surfactant influence on interface roughness and magnetoresistance value in Fe/Cr multilayers. *Thin Solid Films* **2013**, *542*, 199–203. [CrossRef]

57. Chang, C.-L.; Chiou, T.-H.; Chen, P.-H.; Chen, W.-C.; Ho, C.-T.; Wu, W.-Y. Characteristics of TiN/W_2N multilayers prepared using magnetron sputter deposition with dc and pulsed dc powers. *Surf. Coat. Technol.* **2016**, *303*, 25–31. [CrossRef]

58. Saoula, N.; Djerourou, S.; Yahiaoui, K.; Henda, K.; Kesri, R.; Erasmus, R.M.; Comins, J.D. Study of the deposition of Ti/TiN multilayers by magnetron sputtering. *Surf. Interface Anal.* **2010**, *42*, 1176–1179. [CrossRef]

59. Schubert, E.; Frost, F.; Ziberi, B.; Wagner, G.; Neumann, H.; Rauschenbach, B. Ion beam sputter deposition of soft X-ray Mo/Si multilayer mirrors. *J. Vac. Sci. Technol. B Microelectron. Nanometer Struct. Process. Meas. Phenom.* **2005**, *23*, 959–965. [CrossRef]

60. Chiu, P.-K.; Lee, C.-T.; Chiang, D.; Cho, W.-H.; Hsiao, C.-N.; Chen, Y.-Y.; Huang, B.-M.; Yang, J.-R. Conductive and transparent multilayer films for low-temperature TiO_2/Ag/SiO_2 electrodes by E-beam evaporation with IAD. *Nanoscale Res. Lett.* **2014**, *9*, 35. [CrossRef]

61. Kąc, M.; Żukrowski, J.; Toulemonde, M.; Kruk, R.; Tokman, V.; Polit, A.; Zabila, Y.; Dobrowolska, A.; Synashenko, O.; Marszałek, M. Swift iodine ion modification of the structural and magnetotransport properties of Fe/Cr systems. *Nucl. Instrum. Methods Phys. Res. B* **2009**, *267*, 925–930. [CrossRef]

62. Bakonyi, I.; Péter, L. Electrodeposited multilayer films with giant magnetoresistance (GMR): Progress and problems. *Prog. Mater. Sci.* **2010**, *55*, 107–245. [CrossRef]

63. Liu, L.; Zhan, Q.; Yang, H.; Li, H.; Zhang, S.; Liu, Y.; Wang, B.; Tan, X.; Li, R.-W. Magnetostrictive GMR spin valves with composite FeGa/FeCo free layers. *AIP Adv.* **2016**, *6*, 035206. [CrossRef]

64. Zhang, X.G.; Butler, W.H. Large magnetoresistance in bcc Co/MgO/Co and FeCo/MgO/FeCo tunnel junctions. *Phys. Rev. B* **2004**, *70*, 172407. [CrossRef]

65. Sundar, R.S.; Deevi, S.C. Soft magnetic FeCo alloys: Alloy development, processing, and properties. *Int. Mater. Rev.* **2005**, *50*, 157–192. [CrossRef]

66. Reig, C.; Cubells-Beltrán, M.-D. Giant Magnetoresistance (GMR) Magnetometers. In *High Sensitivity Magnetometers*; Grosz, A., Haji-Sheikh, M.J., Mukhopadhyay, S.C., Eds.; Springer International Publishing: Cham, Switzerland, 2017; pp. 225–252.

67. Jin, Z.; Mohd Noor Sam, M.A.I.; Oogane, M.; Ando, Y. Serial MTJ-Based TMR Sensors in Bridge Configuration for Detection of Fractured Steel Bar in Magnetic Flux Leakage Testing. *Sensors* **2021**, *21*, 668. [CrossRef] [PubMed]

68. Coey, J.M.D.; Berkowitz, A.E.; Balcells, L.; Putris, F.F.; Parker, F.T. Magnetoresistance of magnetite. *Appl. Phys. Lett.* **1998**, *72*, 734–736. [CrossRef]

69. Zhang, D.; Liu, Z.; Han, S.; Li, C.; Lei, B.; Stewart, M.P.; Tour, J.M.; Zhou, C. Magnetite (Fe_3O_4) Core−Shell Nanowires: Synthesis and Magnetoresistance. *Nano Lett.* **2004**, *4*, 2151–2155. [CrossRef]

70. Mi, S.; Xie, Y.; Li, Y.; Liu, R.; Liu, X.; Smalyukh, I.I.; Chen, Z. The Effect of Thickness-Tunable ZrO_2 Shell on Enhancing the Tunneling Magnetoresistance of Fe_3O_4 Supraparticles. *Adv. Mater. Interfaces* **2018**, *5*, 1800236. [CrossRef]

71. Liu, E.; Yuan, H.; Kou, Z.; Wu, X.; Xu, Q.; Zhai, Y.; Sui, Y.; You, B.; Du, J.; Zhai, H. Investigation on Spin Dependent Transport Properties of Core-Shell Structural Fe_3O_4/ZnS Nanocomposites for Spintronic Application. *Sci. Rep.* **2015**, *5*, 11164. [CrossRef]

72. Fan, Z.W.; Li, P.; Jiang, E.Y.; Bai, H.L. Evolution of magnetoresistance mechanisms in granular Co/C films with different conduction regimes. *J. Phys. D Appl. Phys.* **2013**, *46*, 065002. [CrossRef]

73. Quan, Z.; Zhang, X.; Liu, W.; Li, X.; Addison, K.; Gehring, G.A.; Xu, X. Enhanced Room Temperature Magnetoresistance and Spin Injection from Metallic Cobalt in Co/ZnO and Co/ZnAlO Films. *ACS Appl. Mater. Interfaces* **2013**, *5*, 3607–3613. [CrossRef]

74. Gerber, A.; Milner, A.; Groisman, B.; Karpovsky, M.; Gladkikh, A.; Sulpice, A. Magnetoresistance of granular ferromagnets. *Phys. Rev. B* **1997**, *55*, 6446–6452. [CrossRef]

75. Gack, N.; Iankevich, G.; Benel, C.; Kruk, R.; Wang, D.; Hahn, H.; Reisinger, T. Magnetotransport Properties of Ferromagnetic Nanoparticles in a Semiconductor Matrix Studied by Precise Size-Selective Cluster Ion Beam Deposition. *Nanomaterials* **2020**, *10*, 2192. [CrossRef] [PubMed]

76. Leveneur, J.; Kennedy, J.; Williams, G.V.M.; Metson, J.; Markwitz, A. Large room temperature magnetoresistance in ion beam synthesized surface Fe nanoclusters on SiO_2. *Appl. Phys. Lett.* **2011**, *98*, 053111. [CrossRef]

77. Zeng, Y.P.; Liu, Z.W.; Yu, H.Y.; Zheng, Z.G.; Zeng, D.C.; Gao, X.S. Large positive room temperature magnetoresistance in nanogranular FeCo–Si–N thin films. *Mater. Lett.* **2013**, *110*, 27–30. [CrossRef]

78. Fukuzawa, H.; Yuasa, H.; Iwasaki, H. CPP-GMR films with a current-confined-path nano-oxide layer (CCP-NOL). *J. Phys. D Appl. Phys.* **2007**, *40*, 1213–1220. [CrossRef]

79. Chaubey, G.S.; Barcena, C.; Poudyal, N.; Rong, C.; Gao, J.; Sun, S.; Liu, J.P. Synthesis and Stabilization of FeCo Nanoparticles. *J. Am. Chem. Soc.* **2007**, *129*, 7214–7215. [CrossRef]

80. Zeng, Y.P.; Liu, Z.W.; Mikmeková, E. Magnetoresistance effects associated with various electric conduction mechanisms in nanostructured [C/FeCo]$_n$ multilayers. *J. Magn. Magn. Mater.* **2017**, *421*, 39–43. [CrossRef]

81. Wang, C.; Xiao, X.; Rong, Y.; Hsu, T.Y. The effect of substrate temperature on the microstructure and tunnelling magnetoresistance of FeCo–Al$_2$O$_3$ nanogranular films. *J. Mater. Sci.* **2006**, *41*, 3873–3879. [CrossRef]

82. Ge, S.-H.; Zhang, Z.-Z.; Lu, Y.-Y.; Li, C.-x.; Run-jin, G. Influence of annealing condition on giant magnetoresistance of FeCo–Cu granular films. *Thin Solid Films* **1997**, *311*, 33–37. [CrossRef]

83. Wang, C.; Xiao, X.; Rong, Y.; Hsu, H.Y. Nanoparticle morphology in FeCo–SiO$_2$ granular films with tunneling giant magnetoresistance. *Mater. Sci. Eng. B* **2007**, *141*, 126–131. [CrossRef]

84. Novoselov, K.S.; Geim, A.K.; Morozov, S.V.; Jiang, D.; Zhang, Y.; Dubonos, S.V.; Grigorieva, I.V.; Firsov, A.A. Electric Field Effect in Atomically Thin Carbon Films. *Science* **2004**, *306*, 666–669. [CrossRef]

85. Wu, H.-C.; Chaika, A.N.; Hsu, M.-C.; Huang, T.-W.; Abid, M.; Abid, M.; Aristov, V.Y.; Molodtsova, O.V.; Babenkov, S.V.; Niu, Y.; et al. Large positive in-plane magnetoresistance induced by localized states at nanodomain boundaries in graphene. *Nat. Commun.* **2017**, *8*, 14453. [CrossRef]

86. Castro Neto, A.H.; Guinea, F.; Peres, N.M.R.; Novoselov, K.S.; Geim, A.K. The electronic properties of graphene. *Rev. Mod. Phys.* **2009**, *81*, 109–162. [CrossRef]

87. Katsnelson, M.I. Graphene: Carbon in two dimensions. *Mater. Today* **2007**, *10*, 20–27. [CrossRef]

88. Bodepudi, S.C.; Singh, A.P.; Pramanik, S. Current-Perpendicular-to-Plane Magnetoresistance in Chemical Vapor Deposition-Grown Multilayer Graphene. *Electronics* **2013**, *2*, 315–331. [CrossRef]

89. Friedman, A.L.; Tedesco, J.L.; Campbell, P.M.; Culbertson, J.C.; Aifer, E.; Perkins, F.K.; Myers-Ward, R.L.; Hite, J.K.; Eddy, C.R.; Jernigan, G.G.; et al. Quantum Linear Magnetoresistance in Multilayer Epitaxial Graphene. *Nano Lett.* **2010**, *10*, 3962–3965. [CrossRef]

90. Gopinadhan, K.; Shin, Y.J.; Yudhistira, I.; Niu, J.; Yang, H. Giant magnetoresistance in single-layer graphene flakes with a gate-voltage-tunable weak antilocalization. *Phys. Rev. B* **2013**, *88*, 195429. [CrossRef]

91. Kisslinger, F.; Ott, C.; Heide, C.; Kampert, E.; Butz, B.; Spiecker, E.; Shallcross, S.; Weber, H.B. Linear magnetoresistance in mosaic-like bilayer graphene. *Nat. Phys.* **2015**, *11*, 650–653. [CrossRef]

92. Hu, J.; Gou, J.; Yang, M.; Omar, G.J.; Tan, J.; Zeng, S.; Liu, Y.; Han, K.; Lim, Z.; Huang, Z.; et al. Room-Temperature Colossal Magnetoresistance in Terraced Single-Layer Graphene. *Adv. Mater.* **2020**, *32*, 2002201. [CrossRef] [PubMed]

93. Shehzad, K.; Xu, Y.; Gao, C.; Duan, X. Three-dimensional macro-structures of two-dimensional nanomaterials. *Chem. Soc. Rev.* **2016**, *45*, 5541–5588. [CrossRef] [PubMed]

94. Jayanthi, S.; Mukherjee, A.; Chatterjee, K.; Sood, A.K.; Misra, A. Tailored nitrogen dioxide sensing response of three-dimensional graphene foam. *Sens. Actuators B* **2016**, *222*, 21–27. [CrossRef]

95. Zhang, Y.; Tang, T.-T.; Girit, C.; Hao, Z.; Martin, M.C.; Zettl, A.; Crommie, M.F.; Shen, Y.R.; Wang, F. Direct observation of a widely tunable bandgap in bilayer graphene. *Nature* **2009**, *459*, 820–823. [CrossRef]

96. Lui, C.H.; Li, Z.; Mak, K.F.; Cappelluti, E.; Heinz, T.F. Observation of an electrically tunable band gap in trilayer graphene. *Nat. Phys.* **2011**, *7*, 944–947. [CrossRef]

97. Xu, G.; Torres, C.M.; Tang, J.; Bai, J.; Song, E.B.; Huang, Y.; Duan, X.; Zhang, Y.; Wang, K.L. Edge Effect on Resistance Scaling Rules in Graphene Nanostructures. *Nano Lett.* **2011**, *11*, 1082–1086. [CrossRef]

98. Murdock, A.T.; Koos, A.; Britton, T.B.; Houben, L.; Batten, T.; Zhang, T.; Wilkinson, A.J.; Dunin-Borkowski, R.E.; Lekka, C.E.; Grobert, N. Controlling the Orientation, Edge Geometry, and Thickness of Chemical Vapor Deposition Graphene. *ACS Nano* **2013**, *7*, 1351–1359. [CrossRef]

99. Sagar, R.R.; Zhang, X.; Xiong, C. Growth of graphene on copper and nickel foils via chemical vapour deposition using ethylene. *Mater. Res. Innov.* **2014**, *18*, S4–S706. [CrossRef]

100. Li, P.; Zhang, Q.; He, X.; Ren, W.; Cheng, H.-M.; Zhang, X.-x. Spatial mobility fluctuation induced giant linear magnetoresistance in multilayered graphene foam. *Phys. Rev. B* **2016**, *94*, 045402. [CrossRef]

101. Rehman Sagar, R.U.; Shehzad, K.; Ali, A.; Stadler, F.J.; Khan, Q.; Zhao, J.; Wang, X.; Zhang, M. Defect-induced, temperature-independent, tunable magnetoresistance of partially fluorinated graphene foam. *Carbon* **2019**, *143*, 179–188. [CrossRef]

102. Liu, Y.; Dong, X.; Chen, P. Biological and chemical sensors based on graphene materials. *Chem. Soc. Rev.* **2012**, *41*, 2283–2307. [CrossRef] [PubMed]

103. Zhang, M.; Li, Y.; Su, Z.; Wei, G. Recent advances in the synthesis and applications of graphene–polymer nanocomposites. *Polym. Chem.* **2015**, *6*, 6107–6124. [CrossRef]

104. Lu, Y.; Goldsmith, B.R.; Kybert, N.J.; Johnson, A.T.C. DNA-decorated graphene chemical sensors. *Appl. Phys. Lett.* **2010**, *97*, 083107. [CrossRef]

105. Krishnan, S.K.; Singh, E.; Singh, P.; Meyyappan, M.; Nalwa, H.S. A review on graphene-based nanocomposites for electrochemical and fluorescent biosensors. *RSC Adv.* **2019**, *9*, 8778–8881. [CrossRef]

106. Stark, W.J. Nanoparticles in Biological Systems. *Angew. Chem. Int. Ed.* **2011**, *50*, 1242–1258. [CrossRef]

107. Xu, H.-L.; Bi, H.; Yang, R.-B. Enhanced microwave absorption property of bowl-like Fe$_3$O$_4$ hollow spheres/reduced graphene oxide composites. *J. Appl. Phys.* **2012**, *111*, 07A522. [CrossRef]

108. Pumera, M. Graphene in biosensing. *Mater. Today* **2011**, *14*, 308–315. [CrossRef]

109. Guo, W.; Zhao, B.; Zhou, Q.; He, Y.; Wang, Z.; Radacsi, N. Fe-Doped ZnO/Reduced Graphene Oxide Nanocomposite with Synergic Enhanced Gas Sensing Performance for the Effective Detection of Formaldehyde. *ACS Omega* **2019**, *4*, 10252–10262. [CrossRef]

110. Wang, D.; Kou, R.; Choi, D.; Yang, Z.; Nie, Z.; Li, J.; Saraf, L.V.; Hu, D.; Zhang, J.; Graff, G.L.; et al. Ternary Self-Assembly of Ordered Metal Oxide−Graphene Nanocomposites for Electrochemical Energy Storage. *ACS Nano* **2010**, *4*, 1587–1595. [CrossRef]

111. Zhang, Y.; Shu, H.; Chang, G.; Ji, K.; Oyama, M.; Liu, X.; He, Y. Facile synthesis of palladium–graphene nanocomposites and their catalysis for electro-oxidation of methanol and ethanol. *Electrochim. Acta* **2013**, *109*, 570–576. [CrossRef]

112. Paredes, J.I.; Villar-Rodil, S.; Fernández-Merino, M.J.; Guardia, L.; Martínez-Alonso, A.; Tascón, J.M.D. Environmentally friendly approaches toward the mass production of processable graphene from graphite oxide. *J. Mater. Chem.* **2011**, *21*, 298–306. [CrossRef]

113. Weiss, R.; Mattheis, R.; Reiss, G. Advanced giant magnetoresistance technology for measurement applications. *Meas. Sci. Technol.* **2013**, *24*, 082001. [CrossRef]

114. Parkin, S.S.P.; More, N.; Roche, K.P. Oscillations in exchange coupling and magnetoresistance in metallic superlattice structures: Co/Ru, Co/Cr, and Fe/Cr. *Phys. Rev. Lett.* **1990**, *64*, 2304–2307. [CrossRef]

115. Gregg, J.F.; Petej, I.; Jouguelet, E.; Dennis, C. Spin electronics-a review. *J. Phys. D Appl. Phys.* **2002**, *35*, R121–R155. [CrossRef]

116. Parkin, S.S.P.; Hayashi, M.; Thomas, L. Magnetic Domain-Wall Racetrack Memory. *Science* **2008**, *320*, 190–194. [CrossRef] [PubMed]

117. Ausserlechner, U. The Optimum Layout for Giant Magneto-Resistive Angle Sensors. *IEEE Sens. J.* **2010**, *10*, 1571–1582. [CrossRef]

118. Wu, S.; Chen, J.; Wu, S. A Rotary Encoder With an Eccentrically Mounted Ring Magnet. *IEEE Trans. Instrum. Meas.* **2014**, *63*, 1907–1915. [CrossRef]

119. Hahn, R.; Schmidt, T.; Slatter, R.; Olberts, B.; Romera, F. Magneto-Resistive Angular Sensors for Space Applications: Results of Breadboard and EQM Testing and Lessons Learned. In Proceedings of the 17th European Space Mechanisms and Tribology Symposium, Hertfordshire, UK, 20–22 September 2017; pp. 20–22.

120. Rempt, R. Scanning with magnetoresistive sensors for subsurface corrosion. *AIP Conf. Proc.* **2002**, *615*, 1771–1778.

121. Wincheski, B.; Simpson, J.; Namkung, M.; Perey, D.; Scales, E.; Louie, R. Development of Giant Magnetoresistive inspection system for detection of deep fatigue cracks under airframe fasteners. *AIP Conf. Proc.* **2002**, *615*, 1007–1014.

122. Gaster, R.S.; Hall, D.A.; Nielsen, C.H.; Osterfeld, S.J.; Yu, H.; Mach, K.E.; Wilson, R.J.; Murmann, B.; Liao, J.C.; Gambhir, S.S.; et al. Matrix-insensitive protein assays push the limits of biosensors in medicine. *Nat. Med.* **2009**, *15*, 1327–1332. [CrossRef] [PubMed]

123. Giebeler, C.; Adelerhof, D.J.; Kuiper, A.E.T.; van Zon, J.B.A.; Oelgeschläger, D.; Schulz, G. Robust GMR sensors for angle detection and rotation speed sensing. *Sens. Actuators A* **2001**, *91*, 16–20. [CrossRef]

124. Rieger, G.; Ludwig, K.; Hauch, J.; Clemens, W. GMR sensors for contactless position detection. *Sens. Actuators A* **2001**, *91*, 7–11. [CrossRef]

125. Hermann, T.M.; Black, W.C.; Hui, S. Magnetically coupled linear isolator. *IEEE Trans. Magn.* **1997**, *33*, 4029–4031. [CrossRef]

126. Rife, J.C.; Miller, M.M.; Sheehan, P.E.; Tamanaha, C.R.; Tondra, M.; Whitman, L.J. Design and performance of GMR sensors for the detection of magnetic microbeads in biosensors. *Sens. Actuators A* **2003**, *107*, 209–218. [CrossRef]

127. Hall, D.A.; Gaster, R.S.; Lin, T.; Osterfeld, S.J.; Han, S.; Murmann, B.; Wang, S.X. GMR biosensor arrays: A system perspective. *Biosens. Bioelectron.* **2010**, *25*, 2051–2057. [CrossRef] [PubMed]

128. Pannetier-Lecoeur, M.; Parkkonen, L.; Sergeeva-Chollet, N.; Polovy, H.; Fermon, C.; Fowley, C. Magnetocardiography with sensors based on giant magnetoresistance. *Appl. Phys. Lett.* **2011**, *98*, 153705. [CrossRef]

129. Shirai, Y.; Hirao, K.; Shibuya, T.; Okawa, S.; Hasegawa, Y.; Adachi, Y.; Sekihara, K.; Kawabata, S. Magnetocardiography Using a Magnetoresistive Sensor Array. *Int. Heart J.* **2019**, *60*, 50–54. [CrossRef] [PubMed]

130. Dixon, R. Magnetic Sensors Report. Available online: https://cdn.ihs.com/www/pdf/1118/ABSTRACT-Magnetic-Sensors%20 Report-2017.pdf (accessed on 27 August 2020).

131. Hoagland, A.S. History of magnetic disk storage based on perpendicular magnetic recording. *IEEE Trans. Magn.* **2003**, *39*, 1871–1875. [CrossRef]

132. Tsang, C.; Chen, M.; Yogi, T.; Ju, K. Gigabit density recording using dual-element MR/inductive heads on thin-film disks. *IEEE Trans. Magn.* **1990**, *26*, 1689–1693. [CrossRef]

133. Heim, D.E.; Fontana, R.E.; Tsang, C.; Speriosu, V.S.; Gurney, B.A.; Williams, M.L. Design and operation of spin valve sensors. *IEEE Trans. Magn.* **1994**, *30*, 316–321. [CrossRef]

134. Maat, S.; Marley, A.C. Physics and Design of Hard Disk Drive Magnetic Recording Read Heads. In *Handbook of Spintronics*; Xu, Y., Awschalom, D.D., Nitta, J., Eds.; Springer Netherlands: Dordrecht, The Netherlands, 2013; pp. 1–45.

135. Parkin, S.S.P.; Roche, K.P.; Samant, M.G.; Rice, P.M.; Beyers, R.B.; Scheuerlein, R.E.; O'Sullivan, E.J.; Brown, S.L.; Bucchigano, J.; Abraham, D.W.; et al. Exchange-biased magnetic tunnel junctions and application to nonvolatile magnetic random access memory (invited). *J. Appl. Phys.* **1999**, *85*, 5828–5833. [CrossRef]

136. Parkin, S.; Xin, J.; Kaiser, C.; Panchula, A.; Roche, K.; Samant, M. Magnetically engineered spintronic sensors and memory. *Proc. IEEE* **2003**, *91*, 661–680. [CrossRef]

137. Tehrani, S. Status and Outlook of MRAM Memory Technology (Invited). In Proceedings of the 2006 International Electron Devices Meeting, San Francisco, CA, USA, 11–13 December 2006; pp. 1–4.

138. Salehi, S.; Fan, D.; Demara, R.F. Survey of STT-MRAM Cell Design Strategies: Taxonomy and Sense Amplifier Tradeoffs for Resiliency. *J. Emerg. Technol. Comput. Syst.* **2017**, *13*, 1–16. [CrossRef]

139. Sbiaa, R.; Piramanayagam, S.N. Recent Developments in Spin Transfer Torque MRAM. *Phys. Status Solidi RRL* **2017**, *11*, 1700163. [CrossRef]

140. Tsukada, K.; Hayashi, M.; Nakamura, Y.; Sakai, K.; Kiwa, T. Small Eddy Current Testing Sensor Probe Using a Tunneling Magnetoresistance Sensor to Detect Cracks in Steel Structures. *IEEE Trans. Magn.* **2018**, *54*, 1–5. [CrossRef]

141. Wang, S.; Wu, Z.; Peng, D.; Li, W.; Zheng, Y. Embedded position estimation using tunnel magnetoresistance sensors for permanent magnet linear synchronous motor systems. *Measurement* **2019**, *147*, 106860. [CrossRef]

142. Reig, C.; Cubells-Beltrán, M.-D.; Ramírez Muñoz, D. Magnetic Field Sensors Based on Giant Magnetoresistance (GMR) Technology: Applications in Electrical Current Sensing. *Sensors* **2009**, *9*, 7919–7942. [CrossRef]

143. Babaytsev, G.V.; Chechenin, N.G.; Dzhun, I.O.; Kozin, M.G.; Makunin, A.V.; Romashkina, I.L. Clusters of Spin Valve Sensors in 3D Magnetic Field of a Label. *Sensors* **2021**, *21*, 3595. [CrossRef]

144. Chen, Z.; Shi, H.; Zhao, C.; Chen, Y. Simulation and Design of DC Sensor Based on Tunnel Magnetoresistance. *J. Phys. Conf. Ser.* **2021**, *1746*, 012023. [CrossRef]

145. Liu, L.; Yang, Y.; Yang, B. Non-contact and high-precision displacement measurement based on tunnel magnetoresistance. *Meas. Sci. Technol.* **2020**, *31*, 065102. [CrossRef]

146. Lee, C.-C.; Yen, Y.-S.; Lai, C.-H. Alignment-Free Sensing Module for Absolute and Incremental Lines in Linear Positioning System Based on Tunneling-Magnetoresistance Sensors. *Sensors* **2021**, *21*, 4137. [CrossRef]

147. Peng, K.-Y.; Chang, J.-Y. Effects of assembly errors on axial positioning accuracy for rotating machinery with magnetoresistance-based magnetic encoders. *Microsyst. Technol.* **2021**, *27*, 2507–2514. [CrossRef]

148. Reig, C.; Pardo, F.; Boluda, J.A.; Vegara, F.; Cubells-Beltrán, M.D.; Sanchis, J.; Abrunhosa, S.; Cardoso, S. Advanced Giant Magnetoresistance (GMR) sensors for Selective-Change Driven (SCD) circuits. In Proceedings of the 2021 13th Spanish Conference on Electron Devices (CDE), Sevilla, Spain, 9–11 June 2021; pp. 58–61.

149. Xu, X.P.; Wang, S.; Liu, T.Z.; Zhu, M.; Wang, J.G. TMR Busbar Current Sensor With Good Frequency Characteristics. *IEEE Trans. Instrum. Meas.* **2021**, *70*, 1–9.

150. Mușuroi, C.; Oproiu, M.; Volmer, M.; Neamtu, J.; Avram, M.; Helerea, E. Low Field Optimization of a Non-Contacting High-Sensitivity GMR-Based DC/AC Current Sensor. *Sensors* **2021**, *21*, 2564. [CrossRef]

151. Lenz, J.; Edelstein, S. Magnetic sensors and their applications. *IEEE Sens. J.* **2006**, *6*, 631–649. [CrossRef]

152. Slatter, R. A6.1-Highly integrated magnetoresistive sensors in aerospace applications. *Proc. SENSOR* **2013**, *2013*, 126–131.

153. Ripka, P.; Janosek, M. Advances in Magnetic Field Sensors. *IEEE Sens. J.* **2010**, *10*, 1108–1116. [CrossRef]

154. Arana, S.; Arana, N.; Gracia, F.J.; Castaño, E. High sensitivity linear position sensor developed using granular Ag–Co giant magnetoresistances. *Sens. Actuators A* **2005**, *123–124*, 116–121. [CrossRef]

155. Stritzke, B.; Brode, C.; Danowski, M. A6.2-Highly flexible absolute integrated encoder system on GMR-basis. *Proc. SENSOR* **2013**, *2013*, 132–137.

156. Albon, C.; Weddemann, A.; Auge, A.; Rott, K.; Hütten, A. Tunneling magnetoresistance sensors for high resolutive particle detection. *Appl. Phys. Lett.* **2009**, *95*, 023101. [CrossRef]

157. Luong, V.; Jeng, J.; Lai, B.; Hsu, J.; Chang, C.; Lu, C. Design of 3-D Magnetic Field Sensor With Single Bridge of Spin-Valve Giant Magnetoresistance Films. *IEEE Trans. Magn.* **2015**, *51*, 1–4. [CrossRef]

158. Zhang, N.; Ye, C.; Peng, L.; Tao, Y. Eddy Current Probe with Three-Phase Excitation and Integrated Array Tunnel Magnetoresistance Sensors. *ITIE* **2021**, *68*, 5325–5336.

159. Ouyang, Y.; He, J.; Hu, J.; Wang, S.X. A Current Sensor Based on the Giant Magnetoresistance Effect: Design and Potential Smart Grid Applications. *Sensors* **2012**, *12*, 15520–15541. [CrossRef] [PubMed]

160. Rifai, D.; Abdalla, A.N.; Ali, K.; Razali, R. Giant Magnetoresistance Sensors: A Review on Structures and Non-Destructive Eddy Current Testing Applications. *Sensors* **2016**, *16*, 298. [CrossRef] [PubMed]

161. Zheng, C.; Zhu, K.; Freitas, S.C.d.; Chang, J.Y.; Davies, J.E.; Eames, P.; Freitas, P.P.; Kazakova, O.; Kim, C.; Leung, C.W.; et al. Magnetoresistive Sensor Development Roadmap (Non-Recording Applications). *IEEE Trans. Magn.* **2019**, *55*, 1–30. [CrossRef]

162. Pelkner, M.; Neubauer, A.; Reimund, V.; Kreutzbruck, M.; Schütze, A. Routes for GMR-Sensor Design in Non-Destructive Testing. *Sensors* **2012**, *12*, 12169–12183. [CrossRef]

163. Bernieri, A.; Ferrigno, L.; Laracca, M.; Rasile, A. Eddy Current Testing Probe Based on Double-Coil Excitation and GMR Sensor. *IEEE Trans. Instrum. Meas.* **2019**, *68*, 1533–1542. [CrossRef]

164. Schotter, J.; Kamp, P.B.; Becker, A.; Pühler, A.; Reiss, G.; Brückl, H. Comparison of a prototype magnetoresistive biosensor to standard fluorescent DNA detection. *Biosens. Bioelectron.* **2004**, *19*, 1149–1156. [CrossRef] [PubMed]

165. Wu, K.; Saha, R.; Su, D.; Krishna, V.D.; Liu, J.; Cheeran, M.C.J.; Wang, J.-P. Magnetic-Nanosensor-Based Virus and Pathogen Detection Strategies before and during COVID-19. *ACS Appl. Nano Mater.* **2020**, *3*, 9560–9580. [CrossRef]

166. Hall, D.A.; Gaster, R.S.; Makinwa, K.A.A.; Wang, S.X.; Murmann, B. A 256 Pixel Magnetoresistive Biosensor Microarray in 0.18 μm CMOS. *IEEE J. Solid-State Circuits* **2013**, *48*, 1290–1301. [CrossRef]

167. Chou, J.; Wu, C.; Kuo, P.; Lai, C.; Nien, Y.; Wu, Y.; Lin, S.; Liao, Y. The Flexible Urea Biosensor Using Magnetic Nanoparticles. *IEEE Trans. Nanotechnol.* **2019**, *18*, 484–490. [CrossRef]

168. Baselt, D.R.; Lee, G.U.; Natesan, M.; Metzger, S.W.; Sheehan, P.E.; Colton, R.J. A biosensor based on magnetoresistance technology. *Biosens. Bioelectron.* **1998**, *13*, 731–739. [CrossRef]

169. Freitas, P.P.; Cardoso, F.A.; Martins, V.C.; Martins, S.A.M.; Loureiro, J.; Amaral, J.; Chaves, R.C.; Cardoso, S.; Fonseca, L.P.; Sebastião, A.M.; et al. Spintronic platforms for biomedical applications. *Lab Chip* **2012**, *12*, 546–557. [CrossRef]

170. Lagaron, J.M.; Cabedo, L.; Cava, D.; Feijoo, J.L.; Gavara, R.; Gimenez, E. Improving packaged food quality and safety. Part 2: Nanocomposites. *Food Addit. Contam.* **2005**, *22*, 994–998. [CrossRef]

171. Ren, C.; Bayin, Q.; Feng, S.; Fu, Y.; Ma, X.; Guo, J. Biomarkers detection with magnetoresistance-based sensors. *Biosens. Bioelectron.* **2020**, *165*, 112340. [CrossRef] [PubMed]

172. Ng, E.; Le, A.K.; Nguyen, M.H.; Wang, S.X. Early Multiplexed Detection of Cirrhosis using Giant Magnetoresistive Biosensors with Protein Biomarkers. *ACS Sens.* **2020**, *5*, 3049–3057. [CrossRef] [PubMed]

173. Adem, S.; Jain, S.; Sveiven, M.; Zhou, X.; O'Donoghue, A.J.; Hall, D.A. Giant magnetoresistive biosensors for real-time quantitative detection of protease activity. *Sci. Rep.* **2020**, *10*, 7941. [CrossRef]

174. Meng, F.; Zhang, L.; Huo, W.; Lian, J.; Jesorka, A.; Shi, X.; Gao, Y. Dynamic Range Expansion of the C-Reactive Protein Quantification with a Tandem Giant Magnetoresistance Biosensor. *ACS Omega* **2021**, *6*, 12923–12930. [CrossRef]

175. Meng, F.; Huo, W.; Lian, J.; Zhang, L.; Shi, X.; Jesorka, A.; Gao, Y. A tandem giant magnetoresistance assay for one-shot quantification of clinically relevant concentrations of N-terminal pro-B-type natriuretic peptide in human blood. *Anal. Bioanal. Chem.* **2021**, *413*, 2943–2949. [CrossRef]

176. Zhu, F.; Li, D.; Ding, Q.; Lei, C.; Ren, L.; Ding, X.; Sun, X. 2D magnetic MoS_2–Fe_3O_4 hybrid nanostructures for ultrasensitive exosome detection in GMR sensor. *Biosens. Bioelectron.* **2020**, *147*, 111787. [CrossRef]

177. Mulvaney, S.P.; Cole, C.L.; Kniller, M.D.; Malito, M.; Tamanaha, C.R.; Rife, J.C.; Stanton, M.W.; Whitman, L.J. Rapid, femtomolar bioassays in complex matrices combining microfluidics and magnetoelectronics. *Biosens. Bioelectron.* **2007**, *23*, 191–200. [CrossRef]

178. Graham, D.L.; Ferreira, H.A.; Freitas, P.P.; Cabral, J.M.S. High sensitivity detection of molecular recognition using magnetically labelled biomolecules and magnetoresistive sensors. *Biosens. Bioelectron.* **2003**, *18*, 483–488. [CrossRef]

179. Srinivasan, B.; Li, Y.; Jing, Y.; Xing, C.; Slaton, J.; Wang, J.-P. A Three-Layer Competition-Based Giant Magnetoresistive Assay for Direct Quantification of Endoglin from Human Urine. *Anal. Chem.* **2011**, *83*, 2996–3002. [CrossRef] [PubMed]

180. Wang, Y.; Wang, W.; Yu, L.; Tu, L.; Feng, Y.; Klein, T.; Wang, J.-P. Giant magnetoresistive-based biosensing probe station system for multiplex protein assays. *Biosens. Bioelectron.* **2015**, *70*, 61–68. [CrossRef]

181. Klein, T.; Wang, W.; Yu, L.; Wu, K.; Boylan, K.L.M.; Vogel, R.I.; Skubitz, A.P.N.; Wang, J.-P. Development of a multiplexed giant magnetoresistive biosensor array prototype to quantify ovarian cancer biomarkers. *Biosens. Bioelectron.* **2019**, *126*, 301–307. [CrossRef] [PubMed]

182. Gao, Y.; Huo, W.; Zhang, L.; Lian, J.; Tao, W.; Song, C.; Tang, J.; Shi, S.; Gao, Y. Multiplex measurement of twelve tumor markers using a GMR multi-biomarker immunoassay biosensor. *Biosens. Bioelectron.* **2019**, *123*, 204–210. [CrossRef]

183. Wu, K.; Klein, T.; Krishna, V.D.; Su, D.; Perez, A.M.; Wang, J.-P. Portable GMR Handheld Platform for the Detection of Influenza A Virus. *ACS Sens.* **2017**, *2*, 1594–1601. [CrossRef] [PubMed]

184. Choi, J.; Gani, A.W.; Bechstein, D.J.B.; Lee, J.-R.; Utz, P.J.; Wang, S.X. Portable, one-step, and rapid GMR biosensor platform with smartphone interface. *Biosens. Bioelectron.* **2016**, *85*, 1–7. [CrossRef]

185. Zhi, X.; Liu, Q.; Zhang, X.; Zhang, Y.; Feng, J.; Cui, D. Quick genotyping detection of HBV by giant magnetoresistive biochip combined with PCR and line probe assay. *Lab Chip* **2012**, *12*, 741–745. [CrossRef] [PubMed]

186. Sharma, P.P.; Albisetti, E.; Massetti, M.; Scolari, M.; La Torre, C.; Monticelli, M.; Leone, M.; Damin, F.; Gervasoni, G.; Ferrari, G.; et al. Integrated platform for detecting pathogenic DNA via magnetic tunneling junction-based biosensors. *Sens. Actuators B* **2017**, *242*, 280–287. [CrossRef]

187. Li, L.; Mak, K.-Y.; Zhou, Y. Detection of HIV-1 antigen based on magnetic tunnel junction sensors. *Chin. Phys. B* **2020**, *29*, 088701. [CrossRef]

188. Wu, Y.; Liu, Y.; Zhan, Q.; Liu, J.P.; Li, R.-W. Rapid detection of Escherichia coli O157:H7 using tunneling magnetoresistance biosensor. *AIP Adv.* **2017**, *7*, 056658. [CrossRef]

189. Kokkinis, G.; Cardoso, S.F.; Cardoso, F.A.; Giouroudi, I. Microfluidics for the Rapid Detection of Pathogens Using Giant Magnetoresistance Sensors. *IEEE Trans. Magn.* **2014**, *50*, 1–4. [CrossRef]

190. Koets, M.; van der Wijk, T.; van Eemeren, J.T.W.M.; van Amerongen, A.; Prins, M.W.J. Rapid DNA multi-analyte immunoassay on a magneto-resistance biosensor. *Biosens. Bioelectron.* **2009**, *24*, 1893–1898. [CrossRef] [PubMed]

191. Mak, A.C.; Osterfeld, S.J.; Yu, H.; Wang, S.X.; Davis, R.W.; Jejelowo, O.A.; Pourmand, N. Sensitive giant magnetoresistive-based immunoassay for multiplex mycotoxin detection. *Biosens. Bioelectron.* **2010**, *25*, 1635–1639. [CrossRef] [PubMed]

192. Ng, E.; Nadeau, K.C.; Wang, S.X. Giant magnetoresistive sensor array for sensitive and specific multiplexed food allergen detection. *Biosens. Bioelectron.* **2016**, *80*, 359–365. [CrossRef]

193. Wang, W.; Wang, Y.; Tu, L.; Klein, T.; Feng, Y.; Li, Q.; Wang, J.-P. Magnetic Detection of Mercuric Ion Using Giant Magnetoresistance-Based Biosensing System. *Anal. Chem.* **2014**, *86*, 3712–3716. [CrossRef]

194. Mu, X.-H.; Liu, H.-F.; Tong, Z.-Y.; Du, B.; Liu, S.; Liu, B.; Liu, Z.-W.; Gao, C.; Wang, J.; Dong, H. A new rapid detection method for ricin based on tunneling magnetoresistance biosensor. *Sens. Actuators B* **2019**, *284*, 638–649. [CrossRef]